Sustainable Chemistry and Pharmacy 35 (2023) 101216

Contents lists available at ScienceDirect

Sustainable Chemistry and Pharmacy

journal homepage: www.elsevier.com/locate/scp

Design approach for the sustainable synthesis of sulfonated biomass-derived hydrochars and pyrochars for the production of 5-(hydroxymethyl)furfural

Domenico Licursi [a, b], Anna Maria Raspolli Galletti [a, b], Benedetta Bertini [a], Leandro Ardemani [c], Nicola Scotti [c], Nicola Di Fidio [a, b], Sara Fulignati [a, b], Claudia Antonetti [a, b, *]

[a] Department of Chemistry and Industrial Chemistry, University of Pisa, Via Giuseppe Moruzzi 13, 56124, Pisa, Italy
[b] Consorzio Interuniversitario Reattività Chimica e Catalisi (CIRCC), Via Celso Ulpiani 27, 70126, Bari, Italy
[c] CNR-SCITEC "Giulio Natta", via Golgi 19, 20133, Milano, Italy

ARTICLE INFO

Handling Editor: Fabio Aricò

Keywords:
Sustainable design approach
Char
Sulfonation
5-(hydroxymethyl)furfural

ABSTRACT

The sustainable synthesis of carbon-based sulfonated acid catalysts from biomass is of paramount importance from the perspective of sustainability. However, the traditional pyrolysis method leads to low solid yields and poor carbon stability. A cascade synthesis is here proposed, combining hydrothermal carbonization and pyrolysis, to produce a "high-quality" carbon-based precursor, followed by its sulfonation to increase the pristine acidity. The proposed multi-step preparation is effective when each step is optimized, primarily the hydrothermal carbonization, which should be carefully optimized. A chemometric approach was employed to optimize the hydrochar synthesis, using microcrystalline cellulose as starting feedstock. The identified optimal reaction conditions were applied to the hydrothermal carbonization of hazelnut shells, which is a more complex but cheaper feedstock, and the obtained hydrochars were pyrolyzed to produce pyrochars. The most promising chars were sulfonated and tested as heterogeneous acid catalysts in the aqueous conversion of fructose to 5-(hydroxymethyl)furfural, a promising platform chemical of great industrial interest, obtaining maximum yields of about 40 mol%. These promising results pave the way for the use of such wastes as efficient acid catalysts for the synthesis of 5-(hydroxymethyl)furfural, contributing to ensure the biomass circular exploitation.

1. Introduction

Lignocellulosic biomass will play a strategic role in many future markets, taking into consideration that a renewable energy share of 32% is binding at the European level by 2030 (Popp et al., 2021). Among the potentially obtainable added-value compounds, acid heterogeneous catalysts are of great relevance, preferring sustainable conditions for the involved synthesis (Chong et al., 2021). In this context, char post-modification by sulfuric acid sulfonation is desirable to improve the acidic properties of the precursor, which can be obtained from biomass through various carbonization methods, such as pyrolysis, gasification, hydrothermal carbonization (HTC) and flash carbonization (Xiong et al., 2018; Cao et al., 2018a, 2023; Zuo et al., 2023; Igboke et al., 2023; Kang et al., 2013). Despite the preference for direct biomass pyrolysis, this choice often results in biochars characterized by low yields and not homoge-

* Corresponding author. Department of Chemistry and Industrial Chemistry, University of Pisa, Via Giuseppe Moruzzi 13, 56124, Pisa, Italy.
E-mail address: claudia.antonetti@unipi.it (C. Antonetti).

https://doi.org/10.1016/j.scp.2023.101216
Received 10 May 2023; Received in revised form 20 July 2023; Accepted 30 July 2023
Available online 2 August 2023

neous morphological and surface properties, often requiring cascade treatments to improve these aspects in the perspective of large-scale production (Zhou et al., 2021; Balasubramaniam et al., 2021; Plachy et al., 2022). As an example, S. Balasubramaniam et al. studied the preparation of sulfonated carbon-based catalyst from the marine biomass *Undaria pinnatifida* using a sequential carbonization method of pyrolysis (1h at 1000°C, under Ar flow) and HTC (3h at 200 °C), followed by modification of the corresponding chars (Balasubramaniam et al., 2021). These ones were tested in the esterification of ethanol with acetic acid, showing better porosity, increased acidity and higher activity than the sulfonated pyrochar or hydrochar alone. On this basis, a multi-step process involving HTC followed by pyrolysis is helpful to produce "high-quality" carbon-based precursors for the synthesis of sulfonated biomass-derived catalysts. HTC promotes the deoxygenation of biomass in water under subcritical conditions. It is a sustainable and cost-effective approach that can be applied to various biomass types, including wet and waste ones, without the need for any pre-drying step (Akkari et al., 2023; Zulfajri et al., 2021; Evcil et al., 2020; Sheng et al., 2019). To date, HTC has been successfully employed on simple monosaccharides and, to a lesser extent, more complex substrates, such as cellulose and/or real biomasses (Akkari et al., 2023; Ischia et al., 2022; Güdücü et al., 2021; Volpe et al., 2020; Pauline and Joseph, 2020). The effect of key reaction parameters, such as temperature, time, type and loading of the biomass feedstock, on the chemical composition and morphology of the produced hydrochars, has been extensively studied adopting univariate approach. Anyway, this evaluation is limiting for the optimal evaluation of the synergy occurring among the involved variables. As highlighted in Table S1 (Supplementary Information), the H/C and O/C molar ratios, as well as the amount of acid groups, are effective output parameters for evaluating the carbonization progress of these carbon materials (Ren et al., 2019; Wang et al., 2018). For their synthesis from cellulose, two different reaction mechanisms have been proposed in the literature (Evcil et al., 2020; Wang et al., 2018), including a) solid-solid pathway and b) soluble pathway, as shown in Fig. 1.

The first one occurs in the solid phase at mild conditions (absence of acid, temperature range 200–280°C, reaction time lower than 3 h) and involves the dehydration and intramolecular condensation reactions of cellulose, leading to the formation of "primary" aromatic hydrochar (pathway a, Fig. 1) (Evcil et al., 2020). On the other hand, the second mechanism occurs in solution (pathway b, Fig. 1) and involves the hydrolysis of cellulose into soluble oligomers, followed by their further hydrolysis into monomeric glucose (Sasaki et al., 1998). Under acidic conditions, glucose can undergo isomerization, dehydration and fragmentation reactions, leading to the formation of several compounds, including 1,6-anhydroglucose, erythrose, furfural, 5-(hydroxymethyl)furfural (HMF), 5-methylfurfural, various acids and aldehydes (Wang et al., 2018).The preferred soluble pathway involves the HMF formation by fructose dehydration, the latter deriving from glucose isomerization (Cao et al., 2015). HMF can undergo *i)* polymerization and/or condensation to form "secondary" hydrochar (pathway b, Fig. 1), characterized by aromatic and furanic units, or *ii)* rehydration to levulinic and formic acids. This soluble pathway is favored under harsher conditions, generally involving temperatures higher than 220°C, reaction times longer than 1 h, high substrate loading (10–20 wt%), and/or suitable acid catalysts (Falco et al., 2011). Dehydration reaction, due to the elimination of hydroxyl groups, and decarboxylation one, caused by the elimination of carboxyl groups, are the two main reactions involved in the hydrochar production (Funke and Ziegler, 2010). Moreover CO_2 formation may occur as a consequence of condensation reactions and the cleavage of intramolecular bonds, in addition to the decomposition of formic acid, which is generally formed in appreciable amounts (Funke and Ziegler, 2010). According to the available literature data on model cellulose (Table S1), the temperature is the most important reaction parameter to modulate yield and properties of the hydrochar. At low temperatures (180–220°C), the yield generally decreases with its increase, because of the improved solubilization of cellulose-derivatives. Further increase of temperature (200–230°C) causes the highest decrease of hydrochar yield. Later at high temperatures (220–260°C), hydrochar yield increases with the raise of temperature and finally, for temperatures higher than 260°C, the hydrochar yield goes back to decrease with the increase of temperature. Continuing with the evaluation of the other independent variables, an increase of the hydrochar yield is generally observed at longer reaction times, whilst a maximum in the hydrochar yield is generally ascertained with an optimal solid/liquid ratio, which should be properly identified with a dedicated optimization study, Regarding the evaluation of the dependent variables, dehydration reactions lead to a decrease in O/C and H/C molar ratios with increasing tem-

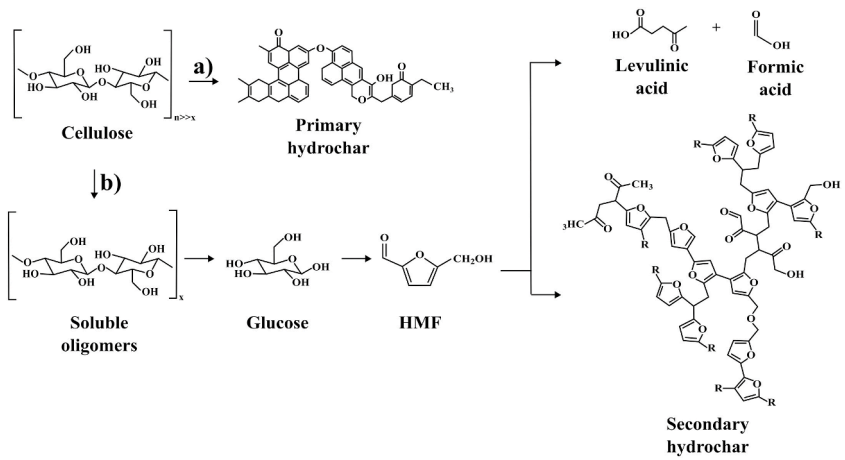

Fig. 1. Hydrochar formation from cellulose according to a) solid-solid pathway and b) soluble pathway.

perature and reaction time (Sheng et al., 2019; Lin et al., 2022), while the content of acidic groups increases with the temperature. For example, these trends were ascertained by N. Saha (Saha et al., 2019), whose best data are summarized in the Supplementary Information (Table S1, runs 25–27). HTC of model compounds, such as simple monosaccharides, leads to high yields in hydrochars, about 50 wt% (Ischia et al., 2022), but these processes are not sustainable for developing industrial applications, due to the high price of starting model feedstocks and the achieved low functionalization degree of hydrochars (Ischia et al., 2022). On the other hand, HTC of real waste biomasses, in particular those of negative economic value, such as agro-food, woody and paper wastes, leads to hydrochars in high yield, with a better functionalization degree, making this process extremely attractive from an industrial perspective (Sharma et al., 2020). The products of any HTC process differ in quantity and composition/physico-chemical properties, depending on the operating conditions. Hence, HTC optimization is highly desirable (Wiedner et al., 2013), preferring a chemiometric approach, thus considering the combined effects of the main reaction parameters on the selected dependent variables. Our study has been firstly focused on microcrystalline cellulose, which is a feedstock of intermediate complexity between soluble monosaccharides and real biomasses. On the basis of this preliminary optimization investigation, hydrochar was prepared from a real lignocellulosic biomass, that is real hazelnut. Both these kinds of hydrochars were subjected to pyrolysis and sulfonation treatment, adopting the typical conditions reported in the literature (Saqib et al., 2018; Gromov et al., 2018), and the resulting sulfonated chars were tested for the aqueous conversion of fructose to HMF, adopting microwave irradiation as heating system. HMF is a versatile key platform-chemical, exploitable for the synthesis of many added-value chemicals, such as bio-fuels, food additives and pharmaceuticals (Fulignati et al., 2022). In this context, HMF can be advantageously oxidized to the higher value-added bioplastic monomer 2,5-furandicarboxylic acid, which is a promising substitute for the petroleum derivative terephthalic acid (Zhang et al., 2023). Remarkably, another valuable HMF conversion possibility is the hydrogenation path, for example aimed at the furanic ring-rearrangement to give cyclopentanones (cyclopentanone and 3-hydroxymethylcyclopentanone) and cyclopentanols (cyclopentanol and 3-hydroxymethylcyclopentanol), both exploitable to produce pharmaceuticals, insecticides, herbicides, and fragrances (Li et al., 2022). The HMF production adopting sulfonated biochars and/or hydrochars has been proposed by some authors (Xiong et al., 2018; Cao et al., 2018a, 2023; Zuo et al., 2023; Igboke et al., 2023; Kang et al., 2013), but none of these systems has been synthesized with a cascade approach, including HTC, followed by pyrolysis and sulfonation, steps, proposed for a better tailoring of the catalytic properties. In this regard, X. Xiong et al. pyrolyzed forestry wood wastes (*Acacia confusa* and *Celtis sinensis*), working at 700°C for 15 h, and performed a sulfonation post-treatment with a 30% wt/v sulfuric acid solution at 150 °C for 24 h. The obtained catalysts were tested in the aqueous conversion of fructose to HMF, achieving the highest HMF yield of 42.3 mol%, employing a high acidity (0.33 meq H^+/g fructose), working at 180°C for 20 min under microwave irradiation (Xiong et al., 2018). Moreover, the authors did not verify the stability of the prepared sulfonated catalysts, not deepening their recyclability, which is instead a highly desirable aspect in the field of heterogeneous catalysis. Finally, it is also important to underline the low adopted initial fructose loading, equal to 4.7 wt%, which is not appropriate for an industrial scale-up. Better results, in terms of HMF molar yield, have been claimed by some authors (Cao et al., 2018a; Zuo et al., 2023; Kang et al., 2013), working in organic solvent/water medium, to minimize the HMF rehydration to levulinic and formic acids, but always employing low substrate loadings. For example, L. Cao et al. synthesized sulfonated biochars by pyrolysis of bread waste (at 700°C for 15 h), followed by a treatment with concentrated sulfuric acid (at 150 °C for 12 h), and the sulfonated pyrochar was used as acid catalyst for the fructose conversion to HMF in dimethylsulfoxide (DMSO)/water (3:1 v/v) solution at 180 °C for 20 min under microwave irradiation (Cao et al., 2018a). The highest HMF yield of 30.4 mol% (calculated on carbon moles of HMF and of bread waste, on the basis of the compositional analysis), was ascertained, which is a high value considering the negative value of the starting material, but it was reached starting from a low substrate loading (4.4 wt%), in combination with a high amount of acid sites (2.42 meq H^+/g bread waste). On the other hand, working in the pure DMSO, the HMF yield of about 90 mol% from fructose was achieved by M. Zuo et al. at 100°C after 4 h, employing sulfonated biochar from the biomass *Larix principis-rupprechtii* synthesized by a pre-carbonization step at 300°C for 1 h under N_2 atmosphere, followed by an activation step with a saturated aqueous solution of $ZnCl_2$ at 25°C for 12 h, then pyrolyzed at 700°C for 1 h under N_2 atmosphere and finally treated with H_2SO_4 at 100°C for 8 h (Zuo et al., 2023). The claimed results are promising, even if the starting fructose loading is again very low (0.7 wt%) and the employed acidity is high (1.9 meq H^+/g fructose). The use of sulfonated hydrochar for HMF production is less investigated in the literature and S. Kang et al. studied its production from inulin, working at 100°C for 1h, in the presence of 1-allyl-3-methylimidazolium chloride as acid catalyst (Kang et al., 2013). Average HMF yields of about 55 mol% were ascertained adopting sulfonated hydrochars deriving from wood meal, cellulose, lignin and xylose after a first HTC treatment at 225–265 °C for 20 h, followed by the sulfonation with concentrated H_2SO_4 at 150°C for 12 h. Anyway, the use of ionic liquid, the long reaction times adopted for the HTC treatment and the impossibility of catalyst recycle does not make this catalyst particularly interesting for the HMF synthesis.

In conclusion, the objectives of the present investigations are to (1) optimize the reaction conditions for the synthesis of hydrochars from cellulose through a chemometric approach; (2) evaluate the properties of the obtained hydrochars and process liquors; (3) use the optimized hydrochar precursor from cellulose and that synthesized from hazelnut shells for the synthesis of acid catalysts through pyrolysis and sulfonation; (4) evaluate the properties of the obtained acid catalysts and (5) test them in the aqueous conversion of fructose to HMF.

2. Materials and methods

2.1. Materials

Microcrystalline cellulose, HMF, potassium bromide, sodium bicarbonate, sodium carbonate, sodium hydroxide 0.1 M and hydrochloric acid 0.1 M were purchased from Sigma-Aldrich and used as-received. Fructose was food-grade and used without any fur-

ther purification. Hazelnut shells of *Tonda Gentile Romana* variety were provided by Stelliferi-Itavex S.p.A., Caprarola, Viterbo (VT), Italy.

2.2. Methods

2.2.1. Experimental design

Response Surface Methodology (RSM) and Face-Centered Central Design (FCCD) were employed for the reaction optimization, by maximizing the hydrochar yield (wt%) as the main response, investigating appropriate ranges of the independent variables. The chosen independent variables are temperature, reaction time and cellulose loading. Their levels were selected starting from preliminary One-Factor-at-a-Time (OFAT) experiments (data not reported). The experimental design required 17 experimental runs, which included 3 replicates of the central point. The software Design-Expert 12 (12.0.1.0) Trial Version (Stat-Ease, Inc., Minneapolis, MN, USA) was adopted to process the results. The data were fitted to the polynomial model and presented in the analysis of variance (ANOVA). The quadratic equation that represents the correlation between independent variables and the response can be expressed by the quadratic polynomial Equation (1):

$$Y = b_0 + b_1X_1 + b_2X_2 + b_3X_3 + b_{11}X_1^2 + b_{22}X_2^2 + b_{33}X_3^2 + b_{12}X_1X_2 + b_{13}X_1X_3 + b_{23}X_2X_3 \quad (1)$$

where Y is the predicted response, b_0 is the constant, b_1, b_2, and b_3 are the linear coefficients, b_{12}, b_{13}, and b_{23} are the cross-product coefficients and b_{11}, b_{22}, and b_{33} are the quadratic coefficients.

2.2.2. Synthesis of hydrochars

In a typical HTC experiment, the selected amount of cellulose was mixed with deionized water (150 mL), with the selected substrate loading (10, 15 or 20 wt%), defined according to the Equation (2):

$$Substrate\ loading\ (wt\%) = \left(\frac{substrate\ (g)}{substrate\ (g) + H2O\ (g)}\right) x\ 100 \quad (2)$$

The slurry was loaded in the 300 mL batch autoclave Parr and heated at the set-point temperature (220, 240, 260 °C) for the selected reaction time (1, 3, 5h), under autogenous pressure. At the end of each HTC run, the autoclave was cooled to room temperature and the solid hydrochar was separated from the aqueous phase by vacuum filtration. The recovered solid hydrochar was washed with 1 L of deionized water, to remove the residual soluble compounds (sugars, HMF, levulinic acid, formic acid and soluble humin precursors) and the hydrochar was dried in an oven at 105 °C overnight. The solid yield was calculated according to the Equation (3):

$$solid\ yield\ (wt\%) = \left(\frac{solid\ from\ HTC\ (g)}{starting\ biomass\ (g)}\right) x100 \quad (3)$$

The hydrochar yield was calculated according to the Equation (4):

$$HTC\ Yield\ (wt\%) = \left(\frac{solid\ from\ HTC\ (g) - cellulose\ in\ the\ solid\ from\ HTC\ (g)}{starting\ biomass\ (g)}\right) x\ 100 \quad (4)$$

where the residual cellulose in the solid from HTC was obtained from thermogravimetric analysis (TGA) performed on the solid recovered after HTC, taking into consideration the weight loss due to cellulose decomposition, calculated according to Equation (5):

$$Residual\ cellulose\ in\ the\ hydrochar = weight\ loss\ due\ to\ cellulose\ decomposition\ by\ TGA\ (wt\%)\ x\ solid\ from\ HTC\ (g) \quad (5)$$

In the same way, hydrochar from hazelnut shells was prepared and labelled HTC-HS, whereas the best hydrochar obtained from cellulose was named HTC-C.

2.2.3. Pyrolysis of hydrochars

A horizontal tubular furnace (Protherm Furnaces, model PTF 12/50/250, Ankara, Turkey) was used for the post-treatment of hydrochars by thermal pyrolysis. In a typical experiment, 10 g of each hydrochar were pyrolyzed within a quartz fixed-bed reactor at 600 °C, employing 500 mL/min of N_2 flow and 10 °C/min as the heating rate, keeping the system at the set-point temperature for 5 min. A thermocouple (type K) was placed on the inner wall of the oven to check the correspondence of the temperature. The inlet and outlet of the pyrolysis reactor were properly heated at 400 °C by heating bands. Primary condensable pyrolytic products flowed through the pyrolysis apparatus into a N_2-bath-cooled trap. At the end of each pyrolysis treatment, the tubular furnace was cooled to room temperature and the solid product was recovered as pyrochar, whereas the bio-oil was retrieved as biphasic (organic-water) mixture and further characterized to get more information about its chemical composition. The obtained pyrochars from cellulose and hazelnut shells were labelled PY-C and PY-HS, respectively, and the pyrochar yield was calculated according to the Equation (6):

$$Pyrochar\ yield\ (wt\%) = \left(\frac{pyrochar\ (g)}{starting\ hydrochar\ (g)}\right) x\ 100 \quad (6)$$

2.2.4. Sulfonation of hydrochars and pyrochars

According to the procedure reported by Gromov et al. (2018), the biomass-derived catalysts have been sulfonated by placing the starting carbon materials in concentrated H_2SO_4 (>98%) in a round-bottom flask, using the concentration of 15 mL of H_2SO_4/g of carbon, under constant stirring. A reflux condenser was added to the flask and the solid was heated under N_2 flow and stirring until 200 °C. After 9 h, the carbon material was washed with water until neutral pH, filtered and dried at 110 °C for one night. After sulfonation, the obtained hydrochars and pyrochars were labelled HTC-C-S and PY-C-S for those deriving from cellulose and HTC-HS-S and PY-HS-S for those from hazelnut shells.

2.2.5. Characterization of the hydrochars and pyrochars

Characterization of the hydrochars and pyrochars was carried out, comparing the data with those of the starting biomass, as reference.

Ultimate analysis of the solid samples was carried out by an automatic LECO TruSpec analyzer. Carbon and hydrogen contents were determined by an infrared spectroscopy detector, whereas nitrogen was determined by a thermal conductivity detector. Lastly, the oxygen content was determined by difference: O (wt%) = 100 (wt%) – C (wt%) – H (wt%) – N (wt%) – S (wt%).

TGA analysis was carried out by a TGA Q500 from TA Instruments. The samples were heated from room temperatures up to 900°C, at a rate of 10°C/min, under a N_2 atmosphere.

Fourier Transform-Infrared Spectroscopy (FT-IR) analysis was performed by a Perkin Elmer Spectrum-Two spectrophotometer. For qualitative purposes, IR spectra were recorded by attenuated total reflection (ATR) mode. In some cases, IR spectra were also acquired by the KBr pellet technique, keeping constant the sample concentration (1.5 mg sample + 180 mg KBr). For the preparation of each pellet, 120 mg of the prepared mixture were employed and each final pellet was characterized by a thickness of 200 ± 10 μm. The acquisition of each spectrum provided 12 scans with a resolution of 8 cm^{-1}.

Scanning electron microscopy (SEM) characterization was carried out by a FEI Quanta 450 FEG scanning electron microscope, equipped with a QUANTAX/EDS analysis system and QUANTAX XFlash Detector 6|10, working under high vacuum conditions (< $6e^{-4}$ Pa). Each sample (about 50 mg) was preliminarily metalized with a thin layer (~10 nm) of conductive material (graphite) to obtain high-quality SEM images.

Specific surface areas were carried out with Brunauer-Emmett-Teller (BET) method using a single-point ThermoQuest Surface Area Analyzer Qsurf S1. Before each measurement, the samples were heated at 150°C for 24 h under a N_2 flow, to remove volatile impurities and trapped moisture.

Boehm's titration of acid sites was carried out according to the procedure described in detail by Tsechansky and Graber (2014). Modified procedure of Boehm's titration, including a pre-treatment aimed at the removal of alkaline species, was carried out only on pyrochars, whilst the traditional Boehm's procedure was adopted for the analysis of hydrochars (Tsechansky and Graber, 2014). Anyway, the sample (1.5 g) was shaken for 24 h in 50 mL of 0.05 N solutions of different bases (NaOH, Na_2CO_3 and $NaHCO_3$). Aliquots of each solution were back-titrated pH-metrically with 0.05 N NaOH after having acidified with an excess of 0.05 N HCl solution (Tsechansky and Graber, 2014). Blank titration (without the solid sample) was performed before the titration, on the same day of the analysis. The acidic functional groups were calculated according to the Equation (7):

$$n\ [mmol] = \frac{n_{HCl}}{n_B} x\,[B]\,x V_B - \left([HCl]\,x V_{HCl} - [NaOH]\,x V_{NaOH}\right) x \frac{V_B}{V_A} \tag{7}$$

where n = number of acid groups [mmol]; $\frac{n_{HCl}}{n_B}$ = stoichiometric factor (1 for NaOH and $NaHCO_3$, 2 for Na_2CO_3); $[B]$ = concentration of added reaction base [mol/L]; V_B = volume of added reaction base [mL]; $[HCl]$ = concentration of HCl [mol/L]; V_{HCl} = volume of HCl [mL]; $[NaOH]$ = NaOH titrant concentration [mol/L] ; V_{NaOH} = NaOH titrant volume [mL]; $\frac{V_B}{V_A}$ = volume of base added initially divided the analyzed volume portion (V_A = 10 mL). To obtain the concentration of total acid sites, expressed in μmol/g, the obtained value from Equation (7) was multiplied by 1000 and divided by the mass (g) of the starting sample.

2.2.6. Characterization of the liquid stream (HTC hydrolysis liquor and bio-oil from pyrolysis)

Hydrolysis liquors from HTC experiments were analyzed by HPLC, employing a Perkin Elmer Flexer Isocratic Platform, equipped with a Benson 2000-0 BP-OA column (300 mm x 7.8 mm) and coupled with 2140 refractive index detector. The 0.005 M H_2SO_4 aqueous solution was adopted as the mobile phase, keeping the column at 60°C, with the flow rate of 0.6 mL/min. The concentrations of the compounds of interest were determined from calibration curves obtained with external standard solutions. According to the involved reaction mechanisms (Cao et al., 2015), glucose, HMF, formic acid and levulinic acid were considered as "glucose-derived compounds", whereas xylose, furfural and acetic acid as "xylose-derived compounds".

The molar yield of glucose and xylose were calculated respect to the moles of the respective units in the polysaccharides (glucan, xylan) in the starting substrate according to the Equations (8) and (9) (Di Fidio et al., 2020):

$$Yield\ in\ glucose\ and\ glucose-derived\ compounds\ (mol\%) = \left(\frac{m_{glucose\ or\ glucose-derived\ compound} x\ 0.90}{m_{substrate}\ x\ G_f}\right) x100 \tag{8}$$

$$Yield\ in\ xylose\ and\ xylose-derived\ compounds\ (mol\%) = \left(\frac{m_{xylose\ or\ xylose-derived\ compound}\ x\ 0.88}{m_{substrate} x\ X_f}\right) x100 \tag{9}$$

where $m_{substrate}$ is the mass of the starting feedstock, 0.90 and 0.88 take into account the stoichiometry and the molecular weights in the hydrolysis of cellulose and hemicellulose to glucose and xylose respectively, and G_f and X_f represent the percentage (wt%) of glucans and xylans in the composition of the starting substrate, equal to 22.9 and 18.6 wt%, respectively for hazelnut shells.

Regarding the chemical analysis of the bio-oil, a preliminary solvent extraction by diethyl ether was carried out (3 times, adopting each time 0.5 g of bio-oil in 3 mL of solvent), and the extract was analyzed by Gas-Chromatography/Mass Spectrometry (GC/MS). For this purpose, a GC-MS (Agilent 7890B-5977A, Agilent Technologies, Santa Clara, CA, USA), outfitted with an HP-5MS column (30 m x 0.25 mm x 0.25 m) was adopted, employing helium as the carrier gas with the flow rate of 1 mL/min (split ratio of 9:1 and split flow of 10 mL/min). The injector and detector were kept at 250 and 280 °C, respectively, and the following temperature program was employed for the chromatographic separation: 60 °C for 2 min; 10 °C/min up to 260 °C, then 260 °C for 3 min and 10 °C/min up to 280 °C. Identification of compounds was performed by comparing experimental mass spectra with those in the NIST Mass Spectral library (NIST14 database; National Institute of Standards and Technology, Maryland, USA).

2.2.7. Characterization of the gaseous stream (non-condensable gases from HTC)

Gaseous compounds (hydrogen, light hydrocarbons and permanent gases) evolved under the harshest reaction conditions (run 2: 260 °C, 5 h, 20 wt% cellulose loading) were collected with a Tedlar bag after cooling of the autoclave and analyzed by a micro-GC Agilent 3000 system. This instrument was equipped with two independent channels based on an injector, a column and a thermal conductivity detector (TCD). The first channel was based on a Molsieve 5A column, using Ar as the mobile phase, resulting appropriate for the separation of hydrogen, oxygen, nitrogen, methane and carbon monoxide. Instead, the second one was based on a PLOT U column, which is effective for the separation of carbon dioxide, ethane, ethylene and acetylene, using He as the carrier gas.

2.2.8. Aqueous conversion of fructose to HMF

The dehydration reactions of fructose to HMF were carried out in a monomodal microwave reactor CEM Discover S-class System. In a standard reaction, aqueous fructose solutions (5 mL, 9 % wt) were charged in the microwave reactor (10 mL) with the proper amount of the selected catalyst. The vessel was placed in the chamber of the MW reactor and heated at 180°C for 20 min under magnetic stirring. At the end of the reaction, the vessel was cooled at room temperature through an external air flow that allows a fast cooling and a portion of the sample was taken for analysis. The sample was filtered through a syringe filter (Whatman 0.45 μm PTFE) and analyzed using a high-performance liquid chromatograph Perkin Elmer Flexer Isocratic Platform equipped with a column Benson 2000-0 BP-OA (300 mm × 7.8 mm) kept at 60°C, employing 0.005 M H_2SO_4 as a mobile phase (flow-rate 0.6 mL/min). The concentrations of the products were determined from calibration curves obtained with standard solutions. Catalytic performances, in terms of fructose conversion, HMF yield and selectivity were calculated in moles % according to Equations (10)–(12).

$$Fructose\ Conversion\ (mol\%) = \left(\frac{initial\ moles_{fructose} - final\ moles_{fructose}}{initial\ moles_{fructose}}\right) x100 \tag{10}$$

$$HMF\ Selectivity\ (mol\%) = \left(\frac{final\ moles_{HMF}}{initial\ moles_{fructose} - final\ moles_{fructose}}\right) x100 \tag{11}$$

$$HMF\ Yield\ (mol\%) = \left(\frac{final\ moles_{HMF}}{initial\ moles_{fructose}}\right) x100 \tag{12}$$

3. Results and discussion

3.1. Optimization of hydrochar synthesis from microcrystalline cellulose

In this research, the optimization of the hydrochar synthesis from microcrystalline cellulose was carried out adopting a multivariate MVAT (multi-variable at time) approach, considering temperature, time and cellulose loading, to synthesize an hydrochar of good quality, in terms of yield and reactivity. This last aspect is mainly defined by the presence of oxygenated groups (-COOH and aromatic/aliphatic -OH), which results of particular interest for applications in the field of acid catalysis (Islam et al., 2022). A preliminary screening of the HTC conditions eligible for the microcrystalline cellulose carbonization was performed according to the One-Factor-At-a-Time approach (data not reported). This screening allowed us to develop a second-order model, known as Central Composite Design (CCD), developed on three levels (Fujiwara and Matsuura, 2020). Based on the preliminary OFAT experiments, the independent variables and the corresponding ranges were defined as follows: temperature (T): 220–260°C, reaction time (t): 1–5 h and starting cellulose loading: 10–20 wt%. The dimensionless and normalized variables, dimensionless temperature (denoted x_1), dimensionless time (denoted x_2) and dimensionless initial cellulose loading (denoted x_3), with variation ranges [-1, 1], were defined as follows:

$$x_1 = 2\cdot[T(°C)-240]/(260-220)$$

$$x_2 = 2\cdot[t(h)-3]/(5-1)$$

$$x_3 = 2\cdot[\text{cellulose loading (wt\%)}-15]/(20-10).$$

Table 1 summarizes the operational conditions, the solid and the HTC yields for the experiments required by the second-order model, expressing the independent variables as dimensional and dimensionless values.

Table 1
Operational conditions, solid and HTC yields, defining the experiments assayed for hydrochar production from cellulose, expressed in terms of dimensional and dimensionless variables.

Run	X_1	X_2	X_3	Temperature [°C]	Time [h]	Cellulose Loading [wt%]	Solid Yield [wt%]	HTC Yield [wt%]
1	0	0	0	240	3	15	**44.5**	**44.5**
2	0	0	0	240	3	15	**45.3**	**45.3**
3	1	−1	1	260	1	20	**45.4**	**45.4**
4	0	0	−1	240	3	10	**41.9**	**41.9**
5	0	0	0	240	3	15	**42.9**	**42.9**
6	−1	1	1	220	5	20	**46.3**	**46.3**
7	0	1	0	240	5	15	**45.5**	**45.5**
8	−1	−1	1	220	1	20	**39.9**	**22.3**
9	−1	−1	−1	220	1	10	**45.5**	**10.4**
10	1	0	0	260	3	15	**44.0**	**44.0**
11	0	0	1	240	3	20	**46.3**	**46.3**
12	1	1	1	260	5	20	**46.3**	**46.3**
13	−1	1	−1	220	5	10	**40.4**	**40.4**
14	1	1	−1	260	5	10	**41.3**	**41.3**
15	−1	0	0	220	3	15	**42.9**	**42.9**
16	0	−1	0	240	1	15	**41.8**	**41.8**
17	1	−1	−1	260	1	10	**40.6**	**40.6**

The primary dependent variable to be monitored was the HTC yield (wt%), which was obtained from the solid yield after the subtraction of the unconverted cellulose contribution, when present. For this purpose, each solid synthesized by runs 1–17 was analyzed by FT-IR spectroscopy and TGA analysis. This approach enabled us to identify the presence of unconverted cellulose in the solids obtained from runs 8 and 9, synthesized under the mildest reaction conditions (Gagić et al., 2018). Fig. S1 shows the FT-IR spectra of these solids, together with the spectrum of a sample synthesized after a longer HTC treatment (the solid from run 6, 220 °C, 5 h, 20 wt%), considering that of the starting cellulose as reference. FT-IR spectra of the hydrochars recovered from HTC of cellulose at short reaction time (runs 8 and 9) are more similar to that of the pristine cellulose, whereas the one originating from the harsher HTC processing (run 6) is completely different, highlighting the occurrence progression of the bulk carbonization. All these samples show an absorption band at about 3300–3400 cm^{-1}, assessed to -OH stretching of water and/or alcohols (Cooke et al., 1986) and another one at about 2900 cm^{-1}, due to aliphatic C-H stretching vibrations (Cooke et al., 1986). Moreover, the hydrochar recovered from run 6 shows distinctive absorption bands, in particular that at about 1700 cm^{-1}, assigned to C = O stretching vibrations of carboxylic groups (Dong et al., 2019), those in the range 1600-1450 cm^{-1}, due to C = C vibrations of aromatic rings (Dong et al., 2019) and that at about 800 cm^{-1}, due to the C-H rocking of aromatic compounds (Liu et al., 2019). On the other hand, the absorption band at about 1050 cm^{-1}, which is typically assigned to C-O stretching of the glycosidic bonds of cellulose (Sheng et al., 2019), is still visible in the hydrochars from runs 8 and 9, confirming an uncompleted cellulose conversion. TGA analyses of hydrochars from runs 8 and 9, shown in Fig. 2, together with that of the starting microcrystalline cellulose, allow us to quantify the residual cellulose in these two solid residues, thus correcting the hydrochar yields.

TG/DTG curves of residues from runs 8 and 9 are very similar, revealing the presence of three degradation steps: the first one, occurring up to about 105 °C, is due to the humidity loss; the second one, occurring between 250 and 400 °C, is attributed to the decomposition of the oxygenated compounds and the residual cellulose, in agreement with that observed for the starting feedstock; lastly, a third thermal degradation step occurs slowly in the wide range 400–900°C, which is ascribed to the decomposition of compounds containing aromatic ring structures, characterized by a high thermo-stability, formed through condensation, polymerization and aromatization reactions during the HTC treatment (Hornung et al., 2021; Ding et al., 2021). On this basis, from the second degradation step, it is possible to quantify cellulose, taking into consideration that the decomposition of oxygenated compounds takes place at around 250°C, thus assuming negligible their contribution in the range 300–400°C, attributed to cellulose (Hornung et al., 2021; Gonnella et al., 2022). Normalization of TGA data on percent basis allowed the quantification of the residual cellulose in these two samples,

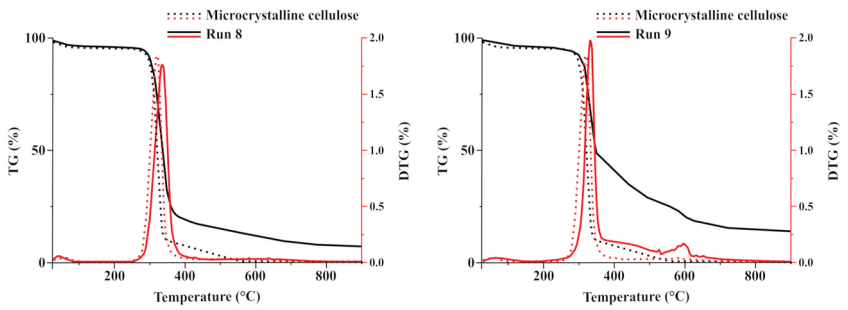

Fig. 2. TG/DTG curves of the solid residues from run 8 (220°C, 1 h, 20 wt%) and run 9 (220°C, 1 h, 10 wt%), in comparison with those of starting microcrystalline cellulose.

amounting to 44.2 and 77.2 wt% for the solids from runs 8 and 9, respectively, giving back the effective hydrochar yields of 22.3 (run 8) and 10.4 (run 9) wt%. To maximize the HTC yield, HTC yields were processed by multivariate analysis, to evaluate simultaneously the interaction of multiple independent variables on the response of interest. Fig. 3 shows the corresponding response surfaces, showing the trend of HTC yield as a function of two of the three independent variables within the domain of interest, keeping constant the third one at the central value.

Fig. 3a shows that hydrochar yield is strongly dependent on the reaction temperature and time. It greatly increases with reaction time at low temperatures (220–230 °C), while at intermediate (240 °C) and higher temperatures (250–260 °C), this increase is less pronounced. At 240 °C, reaction time has a more evident effect on the hydrochar yield than cellulose loading (Fig. 3b). The modest effect of the cellulose loading on the hydrochar yield is also confirmed at intermediate reaction time ($x_2 = 0$, 3 h), where temperature shows a more evident effect than cellulose loading (Fig. 3c). The experimental data were processed by Design Expert software and a second-order polynomial model was developed, to correlate the independent variables with the response, thus obtaining the Equation (13), whereas Table 2 reports the corresponding regression coefficients and the correlation coefficient R^2 for the second-order model.

$$Y = 45.61 + 5.53X_1 + 5.93X_2 + 3.20X_3 - 3.19X_1^2 - 2.99X_2^2 - 2.54X_3^2 - 6.55X_1X_2 - 1.00X_1X_3 - 0.725X_2X_3 \quad (13)$$

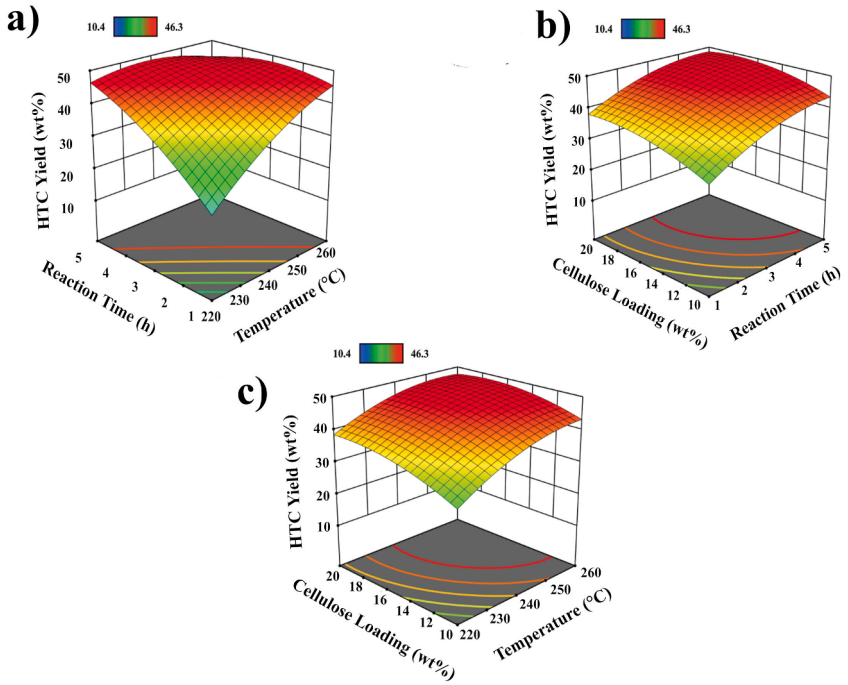

Fig. 3. Three-dimensional (3D) response surfaces: effect of the reaction temperature (°C), reaction time (h) and cellulose loading (wt%) on the hydrochar yield (wt%). (a) Cellulose loading was kept constant at 15 wt% ($x_3 = 0$); (b) reaction temperature was kept constant at 240 °C ($x_1 = 0$); (c) reaction time was kept constant at 3 h ($x_2 = 0$).

Table 2
Regression coefficients of the experimental design (at the 95% of confidence level).

β_0	45.61
β_1	5.53
β_2	5.93
β_3	3.20
β_{12}	−6.55
β_{13}	−1.00
β_{23}	−0.725
β_{11}	−3.19
β_{22}	−2.99
β_{33}	−2.54
R^2	0.9130
Adjusted R^2	0.8011
Adequate precision	10.6111

According to the above linear coefficient values, the main effect on hydrochar yield is ascribed to temperature (β_1) and reaction time (β_2) and, only to a lesser extent, to cellulose loading (β_3). Combined terms have a significant synergistic effect on the response, particularly for the temperature and the reaction time (β_{12}), whereas the other combined effects (temperature with cellulose loading (β_{13}) and reaction time with cellulose loading (β_{23})) result less important. On the other hand, the influence of the quadratic terms (β_{11}, β_{22}, β_{33}) is comparable for all three factors. The high R^2 value (0.9130) is indicative of a close agreement between experimental and predicted values of the hydrochar yield, whereas the R^2 adjusted value is 0.8011 (> 0.6), confirming that the model is significant. In addition, the adequate precision value was higher than 4, highlighting a good signal and confirming that the proposed model well describes the design space. Table 3 reports the results of the analysis of variance (ANOVA) to test the soundness and suitability of the model.

Results were assessed with *p*-value and *F*-value as the main statistical parameters of interest and, in this case, the model has an F-value of 8.16 and a p-value of 0.0057, implying its good significance (Xiros et al., 2017). *F*-values of A, B, C, and AB in Table 3 show that these are significant model terms and, among them, reaction time (B) and temperature (A) have a greater effect, thus confirming the key roles of both these reaction variables on the HTC yield, while cellulose loading has a modest effect, as previously stated.

To identify the optimal experimental conditions, which correspond to the highest HTC yield, the first derivative of the dependent variable (hydrochar yield) as a function of the independent variables (temperature, reaction time and cellulose loading) must be placed equal to zero, according to Equation (14):

$$\frac{\partial Y}{\partial X_1} = \frac{\partial Y}{\partial X_2} = \frac{\partial Y}{\partial X_3} = 0 \tag{14}$$

In this case, Design Expert software proposed 100 solutions, which can be simplified according to practical criteria, such as providing reasonable variations of the reaction temperature at least of 10 °C (Table S2). The final choice of the optimal conditions clearly depends on specific economic considerations that can be made on larger production scales, considering all the involved costs (Paini et al., 2022). At this preliminary level of investigation, the choice of higher temperatures and shorter reaction times is reasonable, also preferring lower cellulose loading to ensure the carbonization progress. On the other hand, also lower temperatures and longer reaction times could be adopted, improving the productivity in hydrochar by preferring a higher cellulose loading. To validate the model, the latter proposal was considered (220 °C, 5 h, 20 wt% of cellulose loading), achieving a good matching between predicted (47.3 wt%) and experimental data (average value 46.7 wt%). These preliminary evaluations are interesting if associated with a careful characterization of the obtained solids, to get more information on the carbonization progress, eventually discriminating among the physico-chemical properties of the hydrochars.

3.2. Characterization of hydrochars from cellulose

The carbonization progress of the solid phase is usefully monitored by the O/C and H/C molar ratios, calculated from ultimate analysis data (Lin et al., 2022), which are also useful for the estimation of the HHVs of the hydrochars (Pauline and Joseph, 2020). These data have been acquired and shown in Table 4, whereas Fig. 4 shows the molar ratios for the synthesized hydrochars according to Van Krevelen diagram, which is used to better monitor the carbonization process (Güleç et al., 2022).

The hydrochars synthesized under milder reaction conditions (runs 8 and 9) are characterized by higher H/C and O/C molar ratios, confirming the limited carbonization, in agreement with the previous characterization (FT-IR and TGA). As a further demonstration, their H/C and O/C molar ratios are similar to those of microcrystalline cellulose. For all the remaining hydrochars, much lower H/C and O/C molar ratios are ascertained, in agreement with the literature data (H/C: 0.8–1.4 and O/C: 0.3–0.5) (Reza et al., 2015). The Van Krevelen diagram shows that dehydration is the dominant path (Wu et al., 2023), followed to a lesser extent by decarboxylation (Wang et al., 2018), thus confirming the carbonization progress. For a more thorough discussion, it is interesting to underline

Table 3
ANOVA for the response surface of the quadratic model.

Source	Sum of Squares	Degree of Freedom	Mean Squares[a]	F-value	*p*-value	Remark
Model	1327.77	9	147.53	8.16	0.0057	significant
A-T	305.81	1	305.81	16.92	0.0045	
B-t	351.65	1	351.65	19.46	0.0031	
C-Loading	102.40	1	102.40	5.67	0.0489	
AB	343.22	1	343.22	18.99	0.0033	
AC	8.00	1	8.00	0.4426	0.5272	
BC	4.20	1	4.20	0.2326	0.6443	
A^2	27.30	1	27.30	1.51	0.2588	
B^2	23.99	1	23.99	1.33	0.2871	
C^2	17.32	1	17.32	0.9580	0.3603	
Residual	126.52	7	18.07			
Lack of Fit	123.53	5	24.71	16.54	0.0580	not significant
Pure Error	2.99	2	1.49			
Cor Total	1454.29	16				

[a] The mean squares values were calculated by dividing the sum of the squares of each variation source by their degrees of freedom, adopting a 95% confidence level to determine the statistical significance in all analyses.

Table 4
Ultimate analysis data, H/C and O/C molar ratios and HHVs of hydrochars deriving from cellulose (hydrochars from runs 1–17). Starting cellulose is reported for comparison (run 0).

Run	Conditions[a] T, t, wt%	C [wt%]	H [wt%]	N [wt%]	S [wt%]	O [wt%]	H/C [mol/mol]	O/C [mol/mol]	HHV[MJ/Kg]
0	Cellulose	40.49	6.22	0.00	0.00	49.29	1.67	0.83	17.8
1	240°C,3h,15 wt%	67.76	4.60	0.01	0.03	27.60	0.81	0.31	26.4
2	240°C,3h,15 wt%	68.42	4.51	0.00	0.00	27.07	0.78	0.30	26.2
3	260°C,1h,20 wt%	68.77	4.56	0.00	0.00	26.67	0.79	0.29	26.7
4	240°C,3h,10 wt%	67.93	4.43	0.00	0.00	27.64	0.78	0.31	26.2
5	240°C,3h,15 wt%	67.94	4.43	0.00	0.00	27.63	0.80	0.29	26.6
6	220°C,5h,20 wt%	65.47	4.66	0.00	0.00	29.87	0.85	0.34	25.4
7	240°C,5h,15 wt%	68.82	4.56	0.00	0.04	26.58	0.79	0.29	26.7
8	220°C,1h,20 wt%	52.31	5.89	0.01	0.03	41.76	1.34	0.60	21.0
9	220°C,1h,10 wt%	44.69	6.10	0.00	0.00	49.21	1.63	0.83	17.9
10	260°C,3h,15 wt%	69.88	4.64	0.02	0.00	25.46	0.79	0.27	27.3
11	240°C,3h,20 wt%	67.64	4.50	0.00	0.00	27.86	0.79	0.31	26.1
12	260°C,5h,20 wt%	70.16	4.68	0.00	0.23	24.93	0.80	0.27	27.5
13	220°C,5h,10 wt%	65.70	4.27	0.01	0.00	30.02	0.77	0.34	25.0
14	260°C,5h,10 wt%	70.05	4.39	0.00	0.00	25.56	0.75	0.27	27.1
15	220°C,3h,15 wt%	66.47	4.37	0.00	0.00	29.16	0.78	0.33	25.4
16	240°C,1h,15 wt%	66.92	4.29	0.01	0.00	28.78	0.76	0.32	25.5
17	260°C,1h,10 wt%	68.88	4.33	0.00	0.00	26.79	0.75	0.29	26.5

[a] The conditions report temperature, reaction time and cellulose loading.

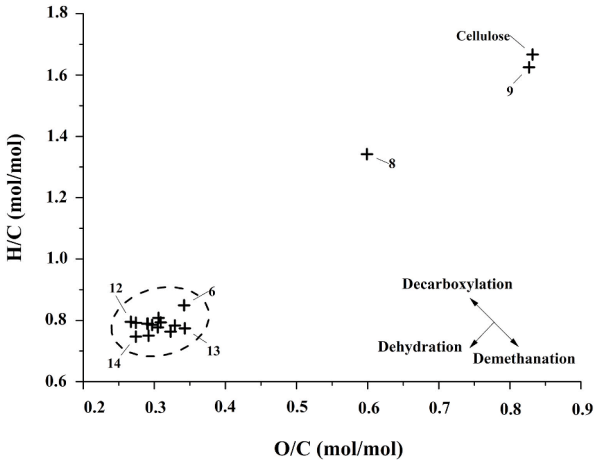

Fig. 4. Van Krevelen diagram of the synthesized hydrochars. Cellulose data are reported for comparison.

some useful comparisons between the input variables and the corresponding H/C and O/C molar ratios and HHV values. In particular, the H/C and O/C molar ratios decrease when the temperature increases, as evidenced by comparing runs 8 and 3, runs 6 and 12, runs 9 and 17, and runs 13 and 14. As for the effect of reaction time, comparing runs 8 and 6 and runs 9 and 13, both molar ratios decrease with an increase in reaction time. In contrast, comparing runs 3 and 12 and runs 17 and 14 highlights a decrease in the O/C molar ratio with increasing reaction time, while the H/C ratio remains almost constant at medium and high temperatures (240–260°C). This trend is attributed to an increase in the contribution of decarboxylation reactions with temperature, which affects the H/C molar ratio more than the dehydration reactions, leading to a nearly constant H/C ratio. Finally, increasing cellulose loading does not significantly affect the O/C ratio but increases the H/C values, as confirmed by comparing runs 17 and 3, runs 14 and 12, and runs 13 and 6. The obtained O/C and H/C molar ratios are in agreement with those available in the literature (Dong et al., 2019). The HHV values are in the range 25.0–27.5 MJ/kg for the hydrochars characterized by complete carbonization. The highest HHV is achieved for the run 12, carried out under the harshest reaction conditions (260 °C, 5 h, 20 wt%, HHV = 27.5 MJ/kg). As shown in Table 4, the HHV values increase with the raise of temperature and reaction time, as a direct consequence of the advanced carbonization, due to the decrease of the oxygen and hydrogen content and the increase of carbon amount (Dong et al., 2019), whereas no significant change of HHVs occurs after variation of the cellulose loading. These hydrochars were further characterized by FT-IR spectroscopy, adopting the KBr technique. As example, Fig. S2 shows the acquired spectra of hydrochar from run 8, as well as those of hydrochars synthesized under more severe conditions (hydrochars from runs 3, 6, 12, and 13), whereas Table 5 reports the results for all the synthesized hydrochars, expressed as ratio (R1) between the area of the absorption band at 1700 cm^{-1} (A_1), associated with C=O stretching vibrations of the carboxylic groups (Dong et al., 2019) and that centered at 1600 cm^{-1} (A_2), associated with C=C stretching vibrations of the aromatic structures (Dong et al., 2019), for better monitoring the progress of the carbonization treatment.

Table 5
R1 ratio (A1 (1700 cm^{-1})/A2 (1600 cm^{-1})) for solids recovered from HTC runs 1–17, at different reaction time, temperature and cellulose loading.

Runs[a]	Temperature [°C]	Reaction Time [h]	Cellulose Loading [wt%]	R1 = $A_{1\ (1700\ cm^{-1})}$ / $A_{2\ (1600cm^{-1})}$
8/6	220	**1/5**	20	0.80/1.24
9/13	220	**1/5**	10	0.41/0.98
3/12	260	**1/5**	20	1.59/1.01
17/14	260	**1/5**	10	1.38/0.99
16/2/7	240	**1/3/5**	15	1.16/1.24/1.42
8/3	**220/260**	1	20	0.80/1.59
9/17	**220/260**	1	10	0.41/1.38
6/12	**220/260**	5	20	1.24/1.01
13/14	**220/260**	5	10	0.98/0.99
15/2/10	**220/240/260**	3	15	1.16/1.24/1.20
9/8	220	1	**10/20**	0.41/0.80
13/6	220	5	**10/20**	0.98/1.24
14/12	260	5	**10/20**	0.99/1.01
17/3	260	1	**10/20**	1.38/1.59
4/2/11	240	3	**10/15/20**	1.35/1.24/1.32

[a] Runs 1, 2 and 5 were performed under the same reaction conditions, thus, run 2 is adopted as representative of their experimental conditions (240°C, 3 h, 15 wt%).

As shown in Table 5, R1 ratio varies from the lowest value of 0.41 (run 9) to the highest one of 1.59 (run 3). In addition to run 9, also run 8 shows a low R1 value, in both cases underlining as the carbonization is initially favored over the formation of carboxylic functionalities. For these samples, the aromatic structures are well-developed, in agreement with the formation of primary hydrochar by solid-phase substrate degradation reactions (Falco et al., 2011). The univariate comparison reported in Table 5 shows that at low temperatures, R1 increases with increasing reaction time, as confirmed, by comparing runs 8 (220 °C, 1 h, 20 wt%, R1 = 0.80) and 6 (220 °C, 5 h, 20 wt%, R1 = 1.24) and by comparing runs 9 (220 °C, 1 h, 10 wt%, R1 = 0.41) and 13 (220 °C, 5 h, 10 wt%, R1 = 0.98). Also at intermediates temperatures, the same trend can be seen by comparing runs 16 (240 °C, 1 h, 15 wt%, R1 = 1.16) and 2 (240 °C, 3 h, 15 wt%, R1 = 1.24) and 7 (240 °C, 5 h, 15 wt%, R1 = 1.42). On the other hand, at high temperature, R1 decreases with reaction time, as evidenced by the comparison between runs 3 (260 °C, 1 h, 20 wt%, R1 = 1.59) and 12 (260 °C, 5 h, 20 wt%, R1 = 1.01) and between runs 17 (260 °C, 1 h, 10 %p/p, R1 = 1.38) and 14 (260 °C, 5 h, 10 %p/p, R1 = 0.99). Regarding the effect of temperature, R1 increases as temperature increases for low reaction time, as evidenced by the comparison between runs 8 (220 °C, 1 h, 20 wt%, R1 = 0.80) and 3 (260 °C, 1 h, 20 wt%, R1 = 1.59), between runs 9 (220 °C, 1 h, 10 wt%, R1 = 0.41) and 17 (260 °C, 1 h, 10 wt%, R1 = 1.38). For intermediate reaction times, the comparison between runs 15 (220 °C, 3 h, 15 wt%, R1 = 1.16) and 2 (240 °C, 3 h, 15 wt%, R1 = 1.24) and 10 (260 °C, 3 h, 15 wt%, R1 = 1.20) underlines an increase of R1 with the increase of temperature up to 240 °C, while the further increase of temperature up to 260 °C causes a R1 decrease. For longer reaction times, the trend of the R1 ratio is opposite or less pronounced, as it can be observed by the comparison between runs 6 (220 °C, 5 h, 20 %, R1 = 1. 24) and 12 (260 °C, 5 h, 20 wt%, R1 = 1.01), while in the comparison between runs 13 (220 °C, 5 h, 10 wt%, R1 = 0.98) and 14 (260 °C, 5 h, 10 wt%, R1 = 0.99) it remains almost constant. Finally, the effect of cellulose loading was considered, showing that R1 increases as the raise of cellulose loading at low temperature, whereas at medium and high temperatures R1 results almost constant with the increment of cellulose loading, as shown from the comparison between runs 9 (220 °C, 1 h, 10 wt%, R1 = 0.41) and 8 (220 °C, 1 h, 20 wt%, R1 = 0.80), between runs 13 (220 °C, 5 h, 10 %p/p, R1 = 0.98) and 6 (220°C, 5h, 20 wt%, R1 = 1.24), between runs 4 (240°C, 3h, 10 wt%, R1 = 1.35) and 2 (240 °C, 3 h, 15 wt%, R1 = 1.24) and 11 (240°C, 3 h, 20 wt%, R1 = 1.32), between runs 14 (260 °C, 5 h, 10 wt%, R1 = 0.99) and 12 (260°C, 5 h, 20 wt%, R1 = 1.01), between runs 17 (260 °C, 1 h, 10 wt%, R1 = 1.38) and 3 (260 °C, 1 h, 20 wt%, R1 = 1.59). In summary, HTC process conducted under more severe conditions, in terms of temperature and/or reaction time, leads to an increase of the R1 ratio. However, above a limited critical value of reaction condition severity, the trend reverses, and the R1 ratio decreases. This behavior can be rationalized taking into consideration than a further increase in the severity of the treatment can cause the degradation of carboxyl groups by decarboxylation reactions (Sheng et al., 2019; Wang et al., 2018; Falco et al., 2011; Wu et al., 2023), which is not desirable for acid applications, such as the investigated HMF formation from fructose dehydration. As reported in the literature, the carboxylic groups, and other oxygenated groups of the catalyst can form strong hydrogen-bonding interactions with fructose, leading to an important synergic effect, by enhancing the performance of the catalysts, enhancing the interaction between the chars and the fructose (Qiao et al., 2015; Qi et al., 2015; Guo et al., 2022), besides the positive contribution of the sulfonic groups for this reaction (Ma et al., 2023; Morales-Leal et al., 2019). Moreover, too high temperatures should be avoided, resulting inappropriate to get appreciable improvements in hydrochar carbonization, which is therefore limited respect to pyrolysis and gasification processes (Lu et al., 2012).

In the perspective of developing applications in acid catalysis (Masoumi et al., 2021), the total acidity determination was carried out by Boehm's titration. The results obtained for the synthesized hydrochars are reported in Table 6, resulting in agreement with those reported in the literature for hydrochars (Saha et al., 2019, 2020).

Runs 1, 2 and 5 were conducted under identical reaction conditions, resulting in similar total acidity values. Thus, run 2 (240°C, 3 h, 15 wt%) was chosen as representative for further analysis, as its value (1112 μmol/g) was closest to the average value obtained from these runs. At low temperatures, acidity increases with reaction time (compare run 8 with 6 and run 9 with 13), which is further

Table 6
Determination of the total acidity of the synthesized hydrochars. Total acidity of the starting cellulose is also reported, for comparison.

Run	Conditions[a] T, t, wt%	Total acid groups [μmol/g]	Run	Conditions[a] T, t, wt%	Total acid groups [μmol/g]
0	*Cellulose*	51	9	220°C, 1h, 10 wt%	518
1	240°C, 3h, 15 wt%	1155	10	260°C, 3h, 15 wt%	1264
2	240°C, 3h, 15 wt%	1112	11	240°C, 3h, 20 wt%	1123
3	260°C, 1h, 20 wt%	1245	12	260°C, 5h, 20 wt%	1209
4	240°C, 3h, 10 wt%	1046	13	220°C, 5h, 10 wt%	1262
5	240°C, 3h, 15 wt%	1087	14	260°C, 5h, 10 wt%	935
6	220°C, 5h, 20 wt%	1384	15	220°C, 3h, 15 wt%	984
7	240°C, 5h, 15 wt%	1208	16	240°C, 1h, 15 wt%	1022
8	220°C, 1h, 20 wt%	986	17	260°C, 1h, 10 wt%	1002

[a] The conditions report temperature, reaction time and cellulose loading.

confirmed at intermediate temperatures (compare run 16 with 2 and 7). However, at high temperatures, a decrease in acidity occurs with longer reaction times (compare run 3 with 12 and run 17 with 14). Regarding the effect of the reaction time, an increase in acidity is observed at higher temperatures and shorter reaction times (compare run 8 with 3 and run 9 with 17), and this trend is also confirmed at intermediate reaction times (compare run 15 with 2 and 10). However, at longer reaction times, acidity decreases with increasing temperature (compare run 6 with 12 and run 13 with 14). Finally, total acidity always increases with cellulose loading for all reaction times (compare run 17 with 3, run 9 with 8, run 14 with 12, run 13 with 6, run 4 with 2, and run 11). Furthermore, the surface morphology of hydrochars was investigated by SEM analysis and some micrographs of hydrochar derived from run 6 is reported in Fig. 5, as an example.

SEM images show the presence of globular structures, constituted by condensed microspheres, known as “humins”, which originate from decompositions of carbohydrates (Ding et al., 2021). Taking into account the mechanisms of hydrochar formation, the cellulosic fraction inside the spherical domains is directly converted into primary hydrochar particles, whereas the fraction in contact with the aqueous phase partially solubilizes, forming particles of secondary hydrochar, which grow progressively, after polymerization/condensation of the liquid-phase intermediates (Falco et al., 2011), resulting visible by the SEM technique. The presence of these (and other) by-products on the surface leads to very low surface areas, which are always lower than 10 m^2/g for all the synthesized hydrochars.

3.3. Characterization of the liquid phase

The liquid phase recovered after separation from the solid hydrochars was analyzed by HPLC to identify and quantify the main components originating from degradation of cellulose, in particular glucose, HMF, furfural, levulinic and formic acids (Cao et al., 2015). Molar yields in these compounds have been evaluated, as well as the pH of the liquors and these data are reported in Table 7.

The presence of glucose, formic acid, levulinic acid, HMF, and furfural in the liquid phase can be used to indirectly evaluate the carbonization progress. Glucose is formed in conditions of backward carbonization, whereas high concentrations of furans and carboxylic acids indicate advanced carbonization (Cao et al., 2015). Runs 8 and 9 show high yields of glucose and lower yields of levulinic acid, confirming a backward carbonization, while runs under severe conditions show high yields of levulinic acid (4.5-10 mol%), indicating an advanced carbonization, in agreement with the recent literature (Lin et al., 2022). The yield of formic acid is highly dependent on the reaction temperature, since it predominantly degrades to CO_2 and H_2. This trend can be observed by comparing run 8 with 3 and run 6 with 12. The yields of the intermediates HMF and furfural under advanced carbonization are low (HMF: < 0.8 mol%, furfural: < 0.7 mol%), whereas these are higher under milder reaction conditions (HMF: 6.5–9.5 mol%, furfural: 1–2.5 mol%).These data are in agreement with the work of H. Lin et al. (2022), underlining that, when more severe reaction conditions are adopted for boosting the carbonization process, HMF and furfural easily degrade. By losing formaldehyde, HMF can also decompose to produce humins and furfural. (Wang et al., 2017). The pH of all the hydrolysates results in the range 2.3–2.9, due to the formation of dissolved acidic organic species. In any case, the pH variation for the obtained hydrolysates is very limited, resulting inappropriate for finely monitoring HTC treatment.

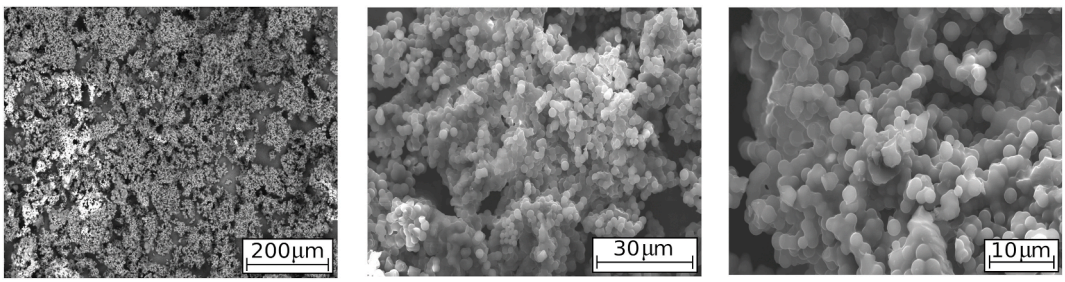

Fig. 5. SEM micrographs of the hydrochar obtained from run 6.

Table 7
Characterization of the liquid phases recovered after HTC of microcrystalline cellulose.

Run	Yield Glucose [mol%]	Yield Formic Acid [mol%]	Yield Levulinic Acid [mol%]	Yield HMF [mol%]	Yield Furfural [mol%]	pH
1	0.1	7.0	5.8	0.2	0.1	2.5
2	n.d.	6.6	3.6	0.3	0.1	2.5
3	n.d.	5.0	3.2	0.2	0.2	2.5
4	0.1	7.0	5.2	0.3	0.2	2.6
5	n.d.	6.5	4.2	0.3	0.1	2.5
6	n.d.	7.8	6.5	0.2	0.1	2.4
7	n.d.	6.5	1.3	0.3	n.d.	2.6
8	18.4	6.5	2.9	6.9	1.8	2.3
9	18.2	7.0	2.2	9.4	2.5	2.6
10	n.d.	5.5	0.5	0.3	0.1	2.6
11	0.1	6.0	4.5	0.2	0.1	2.4
12	n.d.	4.7	n.d.	0.2	n.d.	2.6
13	1.1	9.6	12.6	0.7	0.7	2.5
14	n.d.	6.1	0.7	0.4	0.1	2.9
15	0.5	8.6	11.2	0.5	0.6	2.3
16	0.8	7.2	10.9	0.8	1.3	2.5
17	n.d.	6.1	4.6	0.4	0.4	2.6

n.d. = not detected.

Lastly, the gaseous phase of the reaction conducted under the most severe conditions (run 12, 260 °C, 5 h, 20 wt%) was analyzed by GC analysis. In this case, the HTC processing of cellulose produces a low amount of the non-condensable fraction (H_2 = 0.8 vol%, O_2 = 3.6 vol%, N_2 = 15.3 vol%, CH_4 = 0.1 vol%, CO = 9.4 vol% and CO_2 = 70.8 vol%). The prevalence of CO_2 (70.8 vol%) can be explained considering the occurrence of the decarboxylation path, whereas the low amount of CO (9.4 vol%) and traces of CH_4 (0.1 vol%) and H_2 (0.8 vol%) are in agreement with the literature (Kang et al., 2012). This preliminary information is very useful to demonstrate that, in principle, the proposed HTC treatment can be performed in conditions of good safety.

In conclusion, taking into consideration not only the HTC yield, but also the physico-chemical properties of the hydrochar and its subsequent application, the best reaction conditions were identified at 220°C for 5 h with the cellulose loading of 20 wt%, achieving the HTC yield of 46.3 wt%, comparable to the highest one predicted by the model (47.3 wt%). The hydrochar prepared under the optimal reaction conditions (run 6), named HTC-C, is characterized by H/C and O/C molar ratios of 0.85 and 0.34 respectively, together with the HHV value of 25.4 MJ/kg and the total acidity of 1384 μmol/g, identifying it as a promising solid to be used as catalyst precursor.

3.4. Synthesis and characterization of hydrochars from real biomasses

Once having optimized the hydrochar synthesis from microcrystalline cellulose, the investigation moved towards the synthesis of hydrochar from hazelnut shells (HTC-HS), applying the previously optimized reaction conditions. Hazelnut shell was selected as the waste biomass due to its high abundance in Europe (Ceylan et al., 2022; Saleh et al., 2021), which makes its valorization very important in the perspective of circular economy. At the moment, this waste is mostly used as fuel (Solís et al., 2023) or for recovery of phenolic antioxidants of lignin-source (Di Michele et al., 2021). Regarding the mechanism of hydrochar formation from such real biomasses, it mainly involves the hemicellulose and the cellulose fractions, whereas the lignin one, which is the main component, is more recalcitrant and found as hydrochar, condensed together with humins of carbohydrate source (Cavali et al., 2023). The chemical composition of the adopted hazelnut shells is the following one: cellulose 22.9 wt%, hemicellulose 23.5 wt% (xylan: 18.6 wt%, arabinan: 0.5 wt%, acetyl groups: 4.4 wt%), lignin 37.6 wt%, uronic acids 5.0 wt%, ash 1.4 wt%, extractives 1.4 wt% and other compounds 8.2 wt%. Table 8 summarizes the HTC yields and ultimate analysis data obtained for hazelnut shells. For comparison, the corresponding data of the best hydrochar deriving from cellulose (run 6) HTC-C have also been reported.

The hydrochar yield from hazelnut shells is in agreement with the literature data, resulting in the range 50–60 wt% (Licursi et al., 2017). The high carbon contents of this hydrochar (HTC-HS, Table 8) confirm its occurred carbonization. In detail, the HTC-HS shows a marked decrease of H/C and O/C molar ratios respect to the corresponding starting compound, confirming its lignite-like behavior (Düdder et al., 2016). The occurred carbonization is also confirmed by the corresponding HHV value, equal to 25.6 MJ/kg, which is higher than that of the starting feedstock. The obtained HTC-HS hydrochar was also characterized by FT-IR analysis and the corre-

Table 8
HTC yields, ultimate analysis data, H/C and O/C molar rations and HHVs of hydrochars deriving from HTC of hazelnut shells at 220°C, 5 h, 20 wt% initial loading. For comparison, data from HTC-C (run 6) and the starting feedstocks have been added.

Sample	HTC yield [wt%]	C [wt%]	H [wt%]	N [wt%]	S [wt%]	O [wt%]	H/C [mol/mol]	O/C [mol/mol]	HHV[MJ/Kg]
HTC-HS	56.8	64.07	5.38	0.23	0.17	30.15	1.00	0.35	25.6
HTC-C (run 6)	47.3	65.47	4.66	0.00	0.00	29.87	0.85	0.34	25.4
Hazelnut shells		51.00	5.80	0.20	0.00	43.00	1.36	0.63	20.2
Cellulose		40.49	6.22	0.00	0.00	49.29	1.67	0.83	17.8

sponding spectrum is shown in Fig. S3, together with that of the starting feedstock that results in agreement with that reported in the literature (Hasdemir et al., 2022). For comparison, in the same Fig. S3, the spectra of HTC-C (run 6) and cellulose are shown. The FT-IR spectra of both synthesized hydrochars are very similar to each other, demonstrating the robustness of the HTC treatment also from the real biomass, whereas they result different from those of the starting feedstocks. After carbonization, the band at about 1030 cm^{-1} for the synthesized hydrochars decreased and concurrently new bands appeared, such as that at about 1700 cm^{-1} attributed to C=O stretching vibrations of carboxyl or carbonyl groups (Dong et al., 2019), that at about 1600 cm^{-1} due to C=C stretching of furanic rings and that at about 795 cm^{-1} ascribable to aromatic bending off the plane of the C-H bond (Iroba et al., 2014). Then, the morphology of the synthesized hydrochar from hazelnut shells was investigated by SEM analysis, as reported in Fig. S4, mainly showing the presence of spherical interconnected aggregates, together with isolated particles and the specific surface area was also evaluated, resulting lower than 10 m^2/g. The TGA analysis was further performed and the corresponding thermogram is reported in Fig. S5, together with that of HTC-C (run 6). The thermogram of the hydrochar from hazelnut shells is similar to that deriving from cellulose, showing a first thermal degradation step, due to the release of humidity and volatile substances (4.8 wt%). Then, a second thermal degradation step can be appreciated, assigned to the real thermal degradation of hydrochar (48.7 wt%), in agreement with the available literature data (Hornung et al., 2021). The absence of additional peaks confirms the complete bulk conversion of hemicellulose and cellulose fractions, as expected (Licursi et al., 2017).

The liquid phase recovered from the HTC-HS was analyzed by HPLC, in order to identify and quantify the main components (Table S3). This liquid phase includes levulinic and formic acids as the major identified compounds, originating from the degradation of cellulose fraction, as well as a lower amount of acetic acid, deriving from the hydrolysis of acetyl groups of hemicellulose (Antonetti et al., 2020). Yields in furanic compounds (HMF and furfural) and monosaccharides (glucose and xylose) are low, thus demonstrating a complete conversion of the starting hazelnut shells and, indirectly, the carbonization of the solid phase.

3.5. Synthesis and characterization of pyrochars from cellulose and real biomasses

Slow-pyrolysis is a thermochemical process used for biomass carbonization (Subratti et al., 2021; Wang et al., 2020), producing biochars that have good surface properties, making them useful as adsorbents, fuel cells, and catalysts (Bolan et al., 2022; Huggins et al., 2014; Xiong et al., 2017). For this last use, it is necessary to increase the aromatization degree and the surface area of the native hydrochars (Islam et al., 2022) and pyrolysis post-treatment could be effective also for this purpose. On this basis, pyrolysis post-treatment was carried out on the synthesized hydrochars from cellulose (run 6) and hazelnut shells, obtaining pyrochars, named PY-C and PY-HS respectively. The achieved yields resulted 61.9 and 52.9 wt%, starting from HTC-C (run 6) and HTC-HS, respectively, and the synthesized pyrochars were further characterized by ultimate analysis, FT-IR, SEM and specific surface area. Ultimate data of the synthesized pyrochars are reported in Table 9, together with those of the corresponding hydrochar precursors, for comparison.

The above data related to pyrochars show similar H/C molar ratios, whereas remarkable differences are evident for the O/C molar ratios (from 0.09 to 0.22). However, H/C and O/C molar ratios are in agreement with the available data (H/C: 0.1–0.5 and O/C: 0–0.2) (Hornung et al., 2021). A low O/C molar ratio indicates a high degree of aromatization and a low polarity of the pyrochar, which is highly desirable for traditional high-quality coals. From this perspective, the highest O/C molar ratio ascertained for the PY-C sample highlights its backward carbonization. The decrease of the O/C molar ratio, moving from hydrochars to pyrochars, is related to the occurrence of decarboxalation and dehydration reactions, which occur during the harsher carbonization conditions of the pyrolysis, boosting the decomposition of oxygen-containing compounds and enabling the formation of C-C bonds. The HHVs of the synthesized pyrochars are similar (27.3 and 32.6 MJ/kg for PY-C and PY-HS, respectively) and both higher than those of the corresponding hydrochars (Table 9) and starting compounds (Table 8). The marked increase of HHV values for pyrochars is due to the adopted high pyrolysis temperature, which increases the carbon content and decreases the hydrogen one. These data can be better evaluated according to the Van Krevelen diagram (Fig. 6).

As expected, the above diagram confirms the key role of the dehydration pathway, in agreement with the previous results. FT-IR spectra of the synthesized pyrochars are reported in Fig. S6, showing similar fingerprints and demonstrating the effectiveness of the treatment from different hydrochar precursors. In comparison with hydrochars, pyrochars show a decrease of the absorption band at about 1700 cm^{-1} (C=O stretching of carboxylic groups).On the other hand, both the absorption band at about 1550–1600 cm^{-1} (stretching vibrations of C=C bonds of furanic rings) and that at about 750–820 cm^{-1} (aromatic off-the-plane C-H bending vibrations) increase in the pyrochar samples, confirming that the pyrolysis post-treatment has further improved the carbonization of the solid phase (Iroba et al., 2014). Subsequently, SEM analysis of the pyrochars was performed to examine the surface morphology (Fig. S7), confirming for PY-C the presence of interconnected spheres of relatively uniform sizes, smoother outer surfaces and regular spherical shapes, as in the case of the corresponding hydrochar precursor, whereas for PY-HS it is possible to observe a porous surface, highlighting the presence of spherical humin particles. Specific surface areas of these solids were determined, achieving similar values

Table 9
Ultimate analysis data, H/C and O/C molar rations and HHVs of the synthesized pyrochars (PY-C and PY-HS), together with the corresponding hydrochar precursors.

Sample Name	C [wt%]	H [wt%]	N [wt%]	S [wt%]	O [wt%]	H/C [mol/mol]	O/C [mol/mol]	HHV [MJ/Kg]
PY-C	75.63	2.65	0.00	0.00	21.72	0.42	0.22	27.3
PY-HS	86.38	2.98	0.42	0.04	10.18	0.41	0.09	32.6
HTC-C (run 6)	65.47	4.66	0.00	0.00	29.87	0.85	0.34	25.4
HTC-HS	64.07	5.38	0.23	0.17	30.15	1.00	0.35	25.6

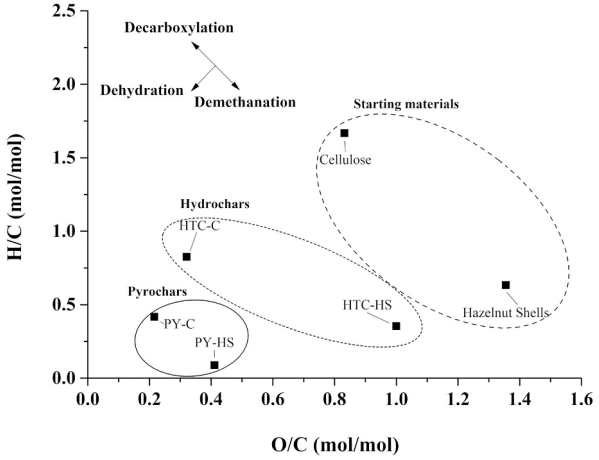

Fig. 6. Van Krevelen diagram of synthesized pyrochars, hydrochars and starting feedstocks (cellulose and hazelnut shells).

(464 m^2/g for PY-C and 397 m^2/g for PY-HS), which are in agreement with biochars obtained from D. Chen et al. (2022), suggesting that the pyrolysis post-treatment of the hydrochar favors the release of volatile trapped compounds, improving its surface properties, as desired for the development of catalytic applications. In addition to the solid phase, the bio-oils recovered from pyrolysis were further characterized by GC-MS analysis and Table S4 summarizes these results, evaluated in terms of normalized areas (%). For a clearer discussion, the components of the bio-oils were classified into seven classes of compounds, acids, aldehydes, aromatics, ethers, furans, ketones and phenols, whose presence is also confirmed by the literature data (Patwardhan et al., 2009). Unidentified compounds are considered as 'other compounds', amounting to 8.4 and 9.6 %, for HTC-C (run 6) and HTC-HS, respectively. Both the obtained bio-oils, from HTC-C (run 6) and HTC-HS, show the presence of aromatics (phenols and furans) as the main compounds (Chen et al., 2022). The analysis of the bio-oil recovered from pyrolysis post-treatment of HTC-HS confirms the presence of phenols and simple monolignols (guaiacol and its derivates, 27.4%), originating from lignin degradation, whereas the furanic compounds were detected together with other furanosidic derivatives, such as 1-(2-furanyl)-ethanone and 5-methylfurfural, in addition to furfural, deriving from the well-known degradation of the cellulosic fraction.

3.6. Functionalization of hydrochars and pyrochars and preliminary test on the acid-catalyzed synthesis of HMF from fructose

In the perspective of proposing the synthesized hydrochars and pyrochars as catalyst precursors for acid-catalyzed reactions, it is essential to determine and increase their surface acidity. This determination was carried out according to Boehm's titration technique, estimating the contributions of total acid groups and that of carboxylic, phenols and lactonic ones (Saha et al., 2020), summarizing the results in Table 10.

The above data highlight a significant difference in acidity between hydrochars (1000–1400 μmol/g) and pyrochars (90–300 μmol/g). Carboxylic groups (500–800 μmol/g) are the main contributors to the total acidity in hydrochars, whose presence was previously identified by FT-IR characterization (Fig. S3), while lactonic groups (350–550 μmol/g) and phenolic ones (50–220 μmol/g) also play an additional role. The presence of lactonic groups is attributed to aromatization and polymerization reactions on the hydrochar surface (Ren et al., 2019). Hydrochars exhibit mild acidic properties, potentially exploitable for acid catalytic applications, but have a low surface area and an irregular morphology, quite similar to the starting precursors. On the other hand, pyrochars have higher surface areas and rudimentary porosity, but show less acidic properties. Thus, pyrochars are better catalyst precursors, in terms of morphological and surface properties, but their acidity should be enhanced. To achieve this goal, sulfonation of the pyrochars PY-C and PY-HS was carried out (Gromov et al., 2018), obtaining PY-C-S and PY-HS-S samples, respectively. Hydrochars HTC-C (run 6) and HTC-HS were also subjected to the same sulfonation treatment, leading to the HTC-C-S and HTC-HS-S samples. All sulfonated chars were characterized and Table 11 shows the results of ultimate analysis, in comparison with the data of the corresponding precursors.

The higher sulfur amount (wt%) in the sulfonated samples confirms the occurred modification. Remarkably, also the oxygen amount is higher in the sulfonated sample, suggesting the presence of more oxygenated functionalities. FT-IR spectra of these samples

Table 10
Total acid, carboxylic, phenols and lactonic groups on the synthesized hydrochars and pyrochars obtained from cellulose and hazelnut shells determined by Boehm's titration.

Sample Name	Total acid groups [μmol/g]	Carboxylic groups [μmol/g]	Phenolic groups [μmol/g]	Lactonic groups [μmol/g]
HTC-C (run 6)	1384	789	53	542
HTC-HS	1052	478	224	350
PY-C	92	4	79	9
PY-HS	289	116	92	81

Table 11
Ultimate analysis data, H/C and O/C molar ratios and HHVs of HTC-C-S and HTC-HS-S and PY-C-S and PY-HS-S. For comparison, data related to the corresponding not sulfonated precursors are reported.

Sample Name	C [wt%]	H [wt%]	N [wt%]	S [wt%]	O [wt%]	H/C [mol/mol]	O/C [mol/mol]	HHV [MJ/Kg]
hydrochars								
HTC-C (run 6)	65.47	4.66	0.00	0.00	29.87	0.85	0.34	25.4
HTC-C-S	**51.84**	**2.51**	**0.02**	**0.96**	**44.56**	**0.58**	**0.65**	**16.6**
HTC-HS	64.07	5.38	0.23	0.17	30.15	1.00	0.35	25.6
HTC-HS-S	**53.81**	**2.37**	**0.20**	**1.12**	**42.50**	**0.53**	**0.59**	**17.3**
pyrochars								
PY-C	75.63	2.65	0.00	0.00	21.72	0.42	0.22	27.3
PY-C-S	**60.93**	**2.60**	**0.04**	**2.07**	**34.36**	**0.51**	**0.42**	**21.0**
PY-HS	86.38	2.98	0.42	0.04	10.18	0.41	0.09	32.6
PY-HS-S	**61.85**	**2.49**	**0.06**	**1.86**	**33.74**	**0.48**	**0.41**	**21.0**

are reported in Figs. S8 and S9, differentiating between hydrochars and pyrochars, respectively. FT-IR spectra of the sulfonated samples differ from those of the corresponding precursors for the presence of the absorption band at 1035 cm^{-1} (SO_3^- stretching vibration), which confirms the occurred sulfonation of the hydrochars/pyrochars (Guo et al., 2012). Moreover, the absorption band at about 1570–1600 cm^{-1} (-C=O stretching vibrations of -COOH groups) was visible in the spectra of sulfonated samples, whereas the more pronounced band at about 3000–3400 cm^{-1}, assigned to the C-OH stretching vibrations and -OH bending vibrations of -COOH groups, indicates the new formation of -COOH, further exploitable for the acid catalysis. The enhanced contribution of the of -COOH groups after sulfonation is reasonably due to the oxidative effect of H_2SO_4 (Cao et al., 2018b; Tamborini et al., 2019).

Furthermore, in order to estimate the contribution of the -SO_3H group, XPS analysis of the samples was performed and the XPS spectrum of PY-C-S example is reported in Fig. S10. XPS data confirm the presence of -SO_3H groups (168 eV). Considering the bulk sulfur content, previously determined by ultimate analysis, it was possible to determine the acid sites due to -SO_3H groups, which was compared with that experimentally obtained according to Boehm's titration (Table 12), due to the increase of total acid groups after sulfonation.

The achieved results from Boehm's titration show for all sulfonated samples a higher acidity (in the range 1400–1700 μmol/g) than that of the corresponding precursors (Table 10). The acidity increase after sulfonation is greater for pyrochars, instead resulting less pronounced for hydrochars. Moreover, the comparison between the two data sets confirms that -SO_3H group contributes to about 20 and 40 wt% of the total acidity for hydrochars and pyrochars, respectively, whereas the remaining contribution is attributed to other additional acidic functionalities (-COOH and -OH groups) (Cao et al., 2018b; Tamborini et al., 2019).

On this basis, the synthesized sulfonated samples (hydrochars and pyrochars) were preliminary tested for the acid-catalyzed hydrothermal synthesis of HMF from fructose, adopting microwave irradiation. The reaction has been extensively studied in the recent literature (Xiong et al., 2018; Cao et al., 2018a; Zuo et al., 2023; Fulignati et al., 2022; Antonetti et al., 2017a, 2017b) and certainly represents a good starting point for a preliminary evaluation of the Brønsted acid properties of our sulfonated systems. For comparison, also the not sulfonated samples, hydrochar and pyrochars, deriving from cellulose and hazelnut shells were tested. This reaction was studied adopting the same reaction conditions previously optimized by us with the sulfonic resin Amberlyst A70 as the Brønsted acid catalyst (Patwardhan et al., 2009), working under microwave irradiation at 180°C for 20 min, with the starting fructose loading of 9 wt%. The amounts of the investigated samples were determined according to their total acidity, adopting the same ratio meq H^+/g of fructose employed previously by us with the Amberlyst A70, equal to 0.031 meq H^+/g fructose (Antonetti et al., 2017b). The obtained data, together with the main features of the investigated samples, are shown in Table 13.

The not sulfonated samples obtained from cellulose, hydrochar (HTC-C (run 6)) and pyrochar (PY-C), were investigated (runs 1 and 3, Table 13). PY-C is characterized by a low acidity, equal to 92 μmol/g, together with a high surface area (464 m^2/g), whereas HTC-C (run 6) shows an interesting acidity of 1384 μmol/g, but a negligible surface area. Therefore, the higher acidity of HTC-C (run 6) enables us to reach increased fructose conversion (65.1 versus 21.5 mol%) and HMF yield (31.0 versus 9.8 mol%), showing comparable performances, in terms of HMF selectivity. Moreover, the huge amount of PY-C necessary to have the selected meq H^+/g fructose ratio can cause mixing limitations, which negatively affect the catalytic performances. In addition to HMF, in the reaction mixtures, levulinic and formic acids were detected, being the rehydration products of HMF in acid conditions and in both runs they re-

Table 12
Total acid groups of the sulfonated samples determined by Boehm's titration and acid sites due to -SO_3H groups based on ultimate analysis.

Sample	Total acid groups [μmol/g][a]	Increase of total acid groups due to sulfonation [μmol/g][b]	Acid sites due to -SO_3H groups on ultimate analysis [μmol/g][c]
HTC-C-S	1688	304	300
HTC-HS-S	1630	578	297
PY-C-S	1390	1298	647
PY-HS-S	1598	1300	581

[a] Determined by Boehm's titration.
[b] calculated as the difference between total acid groups after sulfonation by Boehm's titration and total acid groups before sulfonation by Boehm's titration.
[c] Calculated on the basis of S amount on ultimate analysis in the sample after and before sulfonation.

Table 13
Catalytic conversion of fructose to HMF in water in the presence of not sulfonated hydrochars (HTC-C (run 6) and HTC-HS) and pyrochars (PY-C and PY-HS) and sulfonated hydrochars (HTC-C-S and HTC-HS-S) and pyrochars (PY-C-S and PY-HS-S). Reaction conditions: fructose: 0.5 g, H_2O: 5 mL, 0.031 meq H^+/g fructose, 180°C for 20 min under microwave irradiation.

Run	Catalyst (mg)	Total acid groups (μmol/g)	Specific Surface Area (m^2/g)	Fructose Conversion (mol%)	HMF Selectivity (mol%)	HMF Yield (mol%)	Levulinic acid Yield (mol%)	Formic Acid Yield (mol%)
Initial feedstock: cellulose								
1	HTC-C (run 6) (11.1)	1384	9	65.1	47.6	31.0	0.4	1.3
2	HTC-C-S (9.2)	1688	9	81.8	52.4	42.9	2.4	5.1
3	PY-C (168.5)	92	464	21.5	45.8	9.8	0.3	0.6
4	PY-C-S (11.2)	1390	185	79.7	54.2	43.2	1.4	2.2
Initial feedstock: hazelnul shells								
5	HTC-HS (14.7)	1052	11	36.9	49.1	18.1	0.6	1.1
6	HTC-HS-S (9.5)	1630	11	66.4	44.4	29.5	1.1	1.8
7	PY-HS (53.6)	289	397	27.3	44.2	12.1	0.4	0.7
8	PY-HS-S (9.7)	1598	134	74.4	48.1	35.8	1.1	1.4

sulted low (< 1.5 mol%), confirming the effectiveness of the adopted reaction conditions for HMF synthesis. Then, still starting from cellulose, the corresponding sulfonated systems, HTC-C-S and PY-C-S, were tested (runs 2 and 4, Table 13), showing improved catalytic performances. In fact, HTC-C-S allowed us to obtain the HMF yield of 42.9 mol% with higher fructose conversion and HMF selectivity than those achieved with the corresponding not sulfonated precursor (run 1), due to the increased acidity of the catalyst after the sulfonation treatment, the surface area remaining unchanged. On the other hand, PY-C-S shows comparable results with HTC-C-S, reaching the HMF yield of 43.2 mol%: in this case, its lower acidity (1390 versus 1688 μmol/g) is balanced with a higher surface area (185 versus 9 m^2/g). As expected, in runs 2 and 4, the amounts of levulinic and formic acids are higher than the corresponding ones in runs 1 and 3, as well as the formation of humins, evaluated by higher solid amounts recovered at the end of reactions with sulfonated systems respect to the adopted inizial catalysts amounts (Cao et al., 2018a). When the catalysts deriving from hazelnut shells were employed, the behaviour of the not sulfonated precursors (HTC-HS and PY-HS, runs 5 and 7) is similar to that previously observed for cellulose-derived not sulfonated samples. In fact, HTC-HS (run 5) shows better catalytic performances than PY-HS (run 7), due to higher acidity of the former (1052 versus 289 μmol/g), even if it is characterized by a lower surface area (11 versus 397 m^2/g). Adopting HTC-HS, the HMF yield of 18.1 mol% was ascertained, together with low amounts of HMF rehydration products. Furthermore, also the sulfonated samples from huzelnut shells, HTC-HS-S and PY-HS-S, were tested (runs 6 and 8) and in this case, differently to the corresponding samples from cellulose, PY-HS-S shows higher catalytic performances than HTC-HS-S. Employing the first system in run 8, the HMF yield of 35.8 mol% was obtained in comparison to 29.5 mol% achieved with HTC-HS-S. The two hazelnut shells-derived sulfonated systems are characterized by comparable acidity (1598 and 1630 μmol/g for PY-HS-S and HTC-HS-S, respectively), but different surface area (134 and 11 m^2/g for PY-HS-S and HTC-HS-S, respectively), highlighting that, working with the same acidity, which is the most important parameter, also the surface area and the morphology become important, thus justifying the proposed consecutive multi-step preparation of biomass-derived acid catalysts. The recyclability of the two best systems from cellulose and hazelnut shells (PY-C-S and PY-HS-S), synthesized according the multi-step procedure, was investigated and the obtained results are shown in Fig. 7.

The recycled systems, PY-C-S (run 4) and PY-HS-S (run 8), show a slight decrease of the catalytic performances, obtaining HMF yields of 31.5 and 24.6 mol% respectively, versus 43.2 and 35.8 mol% of the corresponding fresh samples. At the end of the recycling tests, both the catalysts, after simple washing with acetone, were reused again in another recycling test. The catalyst performances were almost completely restored, reaching HMF yields equal to 39.9 and 32.4 mol%, thus highlighting the effectiveness of the simple reactivation procedure. The obtained results with sulfonated pyrochars samples afford HMF yields in the range 35–45 mol%, in agreement with the best data obtained for the same reaction in the literature with sulfonated biochars (Xiong et al., 2018) and with commercial resins (Antonetti et al., 2017b). Regarding sulfonated biochars, the systems prepared from forestry wood waste enabled to achieve the highest HMF yield of 42.3 mol%, employing a high acidity, equal to 0.33 meq H^+/g fructose, at 180°C for 20 min under microwave irradiation (Xiong et al., 2018). Furthermore, the authors report the occurrence of secondary reactions arising from the reaction intermediates and the stability of the synthesized sulfonated catalysts was not verified and discussed. Moreover, it is also important to underline that the initial fructose loading employed, which was only 4.7 wt%, is not feasible for industrial-scale applications. Regarding the comparison with commercial acid resins, our results are comparable with those reached, under the same reaction conditions, with Amberlyst-70, thus confirming the effectiveness of the synthesized sulfonated samples which could be employed in a wider temperature range respect to organic resins. These results open the way to extend the proposed multi step preparation also to waste resources, to verify their promising potential as acid catalysts for biomass circular exploitation.

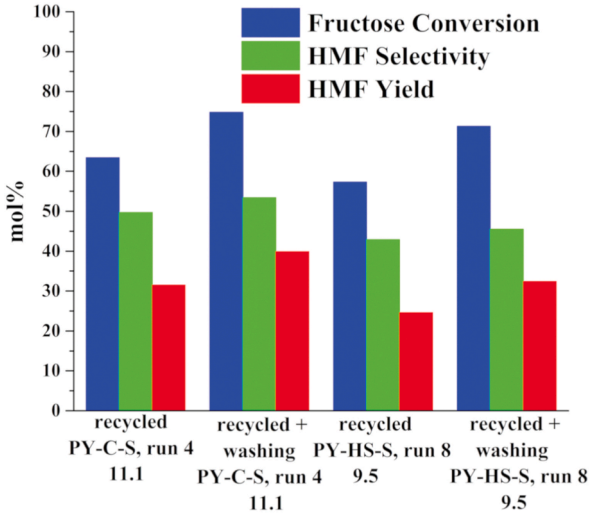

Fig. 7. Catalytic results for the conversion of fructose to HMF in water in the presence of recycled PY-C-S (run 4), PY-HS-S (run 8) and recycled and washing treatment of PY-C-S (run 4) and PY-HS-S (run 8). Reaction conditions: fructose: 0.5 g, H_2O: 5 mL, 0.031 meq H^+/g fructose,180°C for 20 min under microwave irradiation.

4. Conclusions

In this paper, a cascade preparation made up of hydrothermal carbonization followed by pyrolysis, has been proposed to produce a "high-quality" carbon-based precursor, increasing the solid yield and improving its morphological and surface properties. The subsequent sulfonation step was performed to obtain the final acid catalyst. The proposed multi-step preparation results effective when each step is optimized, in particular the hydrochar synthesis, which was optimized through a chemometric approach, to consider the synergistic contribution of the main reaction parameters. The best reaction conditions were selected not only on the basis of the hydrochar yield, but also considering the tailored production of a reactive hydrochar to be suitable for further modification/functionalization, whereas the liquid phase allowed us to indirectly monitor the carbonization progress. Thus, optimization study was performed on microcrystalline cellulose and then applied to the hazelnut shells, as a real biomass feedstock. The obtained hydrochars were characterized and the best ones were pyrolyzed to obtain pyrochars. Then, the most promising hydrochars and pyrochars were sulfonated and successfully tested as heterogeneous acid catalysts in the aqueous conversion of fructose to HMF, reaching very interesting yield (40 mol%), thus justifying their use as green acid catalysts, well-exploitable in the perspective of circular economy.

Authorship statements

Domenico Licursi: Methodology, Investigation, Data Curation, Writing-Original Draft preparation. Anna Maria Raspolli Galletti: Methodology, Resources, Writing-Reviewing and Editing. Benedetta Bertini: Investigation. Leandro Ardemani: Investigation. Nicola Scotti: Methodology, Data Curation. Nicola Di Fidio: Validation, Formal Analysis. Sara Fulignati: Validation, Formal Analysis. Claudia Antonetti: Conceptualization, Data Curation, Writing-Original Draft preparation, Writing-Reviewing and Editing, Supervision, Funding acquisition.

Declaration of competing interest

The authors declare that they have no known competing financial interests or personal relationships that could have appeared to influence the work reported in this paper.

Data availability

The authors are unable or have chosen not to specify which data has been used.

Acknowledgments

The authors are grateful to Italian Ministero dell'Istruzione, dell'Università e della Ricerca for the financial support provided through the PRIN 2020 LEVANTE project "LEvulinic acid Valorization through Advanced Novel TEchnologies" (Progetti di Ricerca di Rilevante Interesse Nazionale Bando 2020, 2020CZCJN7).

Appendix A. Supplementary data

Supplementary data to this article can be found online at https://doi.org/10.1016/j.scp.2023.101216.

References

Akkari, I., Spessato, L., Graba, Z., Bezzi, N., Kaci, M.M., 2023. A sustainably produced hydrochar from pomegranate peels for the purification of textile contaminants in an aqueous medium. Sustain. Chem. Pharm. 31, 100924. https://doi.org/10.1016/j.scp.2022.100924.

Antonetti, C., Melloni, M., Licursi, D., Fulignati, S., Ribechini, E., Rivas, S., Parajó, J.C., Cavani, F., Raspolli Galletti, A.M., 2017a. Microwave-assisted dehydration of fructose and inulin to HMF catalyzed by niobium and zirconium phosphate catalysts. Appl. Catal., B 206, 364–377. https://doi.org/10.1016/j.apcatb.2017.01.056.

Antonetti, C., Raspolli Galletti, A.M., Fulignati, S., Licursi, D., 2017b. Amberlyst A-70: a surprisingly active catalyst for the MW assisted dehydration of fructose and inulin to HMF in water. Catal. Commun. 97, 146–150.

Antonetti, C., Gori, S., Licursi, D., Pasini, G., Frigo, S., López, M., Parajó, J.C., Raspolli Galletti, A.M., 2020. One-pot alcoholysis of the lignocellulosic *Eucalyptus nitens* biomass to *n*-butyl levulinate, a valuable additive for diesel motor. Catalysts 10, 509–530. https://doi.org/10.3390/catal10050509.

Balasubramaniam, S., Ninomiya, S., Sasaki, M., Quitain, A., Kida, T., Saldana, M.D.A., 2021. Carbon-based solid acid catalyst derived from Undaria pinnatifida and its application in esterification. Algal Res. 55, 102272. https://doi.org/10.1016/j.algal.2021.102272.

Bolan, N., Hoang, S.A., Beiyuan, J., Gupta, S., Hou, D., Karakoti, A., Joseph, S., Jung, S., Kim, K.H., Kirkham, M.B., Kua, H.W., Kumar, M., Kwon, E.E., Ok, Y.S., Perera, V., Rinklebe, J., Shaheen, S.M., Sarkar, B., Sarmah, A.K., Singh, G., Tsang, D.C.W., Vikrant, K., Vithanage, M., Vinu, A., Wang, H., Wijesekara, H., Yan, Y., Younis, S.A., Van Zwieten, L., 2022. Multifunctional applications of biochar beyond carbon storage. Int. Mater. Rev. 67, 150–200. https://doi.org/10.1080/09506608.2021.1922047.

Cao, X., Peng, X., Sun, S., Zhong, L., Chen, W., Wang, S., Sun, R.C., 2015. Hydrothermal conversion of xylose, glucose, and cellulose under the catalysis of transition metal sulfates. Carbohydr. Polym. 118, 44–51. https://doi.org/10.1016/j.carbpol.2014.10.069.

Cao, L., Yu, I.K.M., Chen, S.S., Tsang, D.C.W., Wang, L., Xiong, X., Zhang, S., Ok, Y.S., Kwon, E.E., Song, H., Poon, C.S., 2018a. Production of 5-hydroxymethylfurfural from starch-rich food waste catalyzed by sulfonated biochar. Bioresour. Technol. 252, 76–82. https://doi.org/10.1016/j.biortech.2017.12.098.

Cao, L., Yu, I.K.M., Chen, S.S., Tsang, D.C.W., Wang, L., Xiong, X., Zhang, S., Ok, Y.S., Kwon, E.E., Song, H., Poon, C.S., 2018b. Production of 5-hydroxymethylfurfural from starch-rich food waste catalyzed by sulfonated biochar. Bioresour. Technol. 252, 76–82. https://doi.org/10.1016/j.biortech.2017.12.098.

Cao, M., Lu, M., Yin, H., Zhu, Q., Xing, K., Ji, J., 2023. Effect of hemicellulose extraction pretreatment on sulfonated corncob biochar for catalytic biodiesel production. J. Environ. Chem. Eng. 11, 109058. https://doi.org/10.1016/j.jece.2022.109058.

Cavali, M., Libardi, Jr, N., de Sena, J.D., Woiciechowski, A.L., Soccol, C.R., Filho, P.B., Bayard, R., Benbelkacem, H., de Castilhos, Jr, A.B., 2023. A review on hydrothermal carbonization of potential biomass wastes, characterization and environmental applications of hydrochar, and biorefinery perspectives of the process. Sci. Total Environ. 857, 159627. https://doi.org/10.1016/j.scitotenv.2022.159627.

Ceylan, F.D., Adrar, N., Bolling, B.W., Capanoglu, E., 2022. Valorisation of hazelnut by-products: current applications and future potential. Biotechnol. Genet. Eng. Rev. https://doi.org/10.1080/02648725.2022.2160920. (in press). .

Chen, D., Cen, K., Zhuang, X., Gan, Z., Zhou, J., Zhang, Y., Zhang, H., 2022. Insight into biomass pyrolysis mechanism based on cellulose, hemicellulose, and lignin: evolution of volatiles and kinetics, elucidation of reaction pathways, and characterization of gas, biochar and bio-oil. Combust. Flame 242, 112142. https://doi.org/10.1016/j.combustflame.2022.112142.

Chong, C.C., Cheng, Y.W., Lam, M.L., Setiabudi, H.D., Vo, D.V.N., 2021. State-of-the-Art of the synthesis and applications of sulfonated carbon-based catalysts for biodiesel production: a review. Energy Technol. 9, 2100303. https://doi.org/10.1002/ente.202100303.

Cooke, N.E., Fuller, O.M., Gaikwad, R.P., 1986. FT-i.r. spectroscopic analysis of coals and coal extracts. Fuel 65, 1254–1260. https://doi.org/10.1016/0016-2361(86)90238-3.

Di Fidio, N., Raspolli Galletti, A.M., Fulignati, S., Licursi, D., Liuzzi, F., De Bari, I., Antonetti, C., 2020. Multi-step exploitation of raw *Arundo donax* L. for the selective synthesis of second-generation sugars by chemical and biological route. Catalysts 10, 79–101. https://doi.org/10.3390/catal10010079.

Di Michele, A., Pagano, C., Allegrini, A., Blasi, F., Cossignani, L., Raimo, E.D., Faieta, M., Oliva, E., Pittia, P., Primavilla, S., Sergi, M., Vicino, C., Ricci, M., Schirone, B., Perioli, L., 2021. Hazelnut shells as source of active ingredients: extracts preparation and characterization. Molecules 26, 6607–6624. https://doi.org/10.3390/molecules26216607.

Ding, Z., Zhang, L., Mo, H., Chen, Y., Hu, X., 2021. Microwave-assisted catalytic hydrothermal carbonization of *Laminaria japonica* for hydrochars catalyzed and activated by potassium compounds. Bio Technol. 341, 125835. https://doi.org/10.1016/j.biortech.2021.125835.

Dong, X., Guo, S., Wang, H., Wang, Z., Gao, X., 2019. Physicochemical characteristics and FTIR-derived structural parameters of hydrochar produced by hydrothermal carbonisation of pea pod (*Pisum sativum* Linn.) waste. Biomass Convers. Biorefin. 9, 531–540. https://doi.org/10.1007/s13399-018-0363-1.

Düdder, H., Wütscher, A., Stoll, R., Muhler, M., 2016. Synthesis and characterization of lignite-like fuels obtained by hydrothermal carbonization of cellulose. Fuel 171, 54–58. https://doi.org/10.1016/j.fuel.2015.12.031.

Evcil, T., Simsir, H., Ucar, S., Tekin, K., Karagoz, S., 2020. Hydrothermal carbonization of lignocellulosic biomass and effects of combined Lewis and Brønsted acid catalysts. Fuel 279, 118458. https://doi.org/10.1016/j.fuel.2020.118458.

Falco, C., Baccile, N., Titirici, M.M., 2011. Morphological and structural differences between glucose, cellulose and lignocellulosic biomass derived hydrothermal carbons. Green Chem. 13, 3273. https://doi.org/10.1039/c1gc15742f.

Fujiwara, K., Matsuura, S., 2020. Prediction variance of a central composite design with missing observation. Commun. Stat. Theor. Methods 49, 6016–6031. https://doi.org/10.1080/03610926.2019.1625925.

Fulignati, S., Licursi, D., Di Fidio, N., Antonetti, C., Raspolli Galletti, A.M., 2022. Novel challenges on the catalytic synthesis of 5-hydroxymethylfurfural (HMF) from real feedstocks. Catalysts 12, 1664. https://doi.org/10.3390/catal12121664.

Funke, A., Ziegler, F., 2010. Hydrothermal carbonization of biomass: a summary and discussion of chemical mechanisms for process engineering. Biofuels, Bioprod. Bioref. 4, 160–177. https://doi.org/10.1002/bbb.198.

Gagić, T., Perva-Uzunalić, A., Knez, Ž., Škerget, M., 2018. Hydrothermal degradation of cellulose at temperature from 200 to 300 °C. Ind. Eng. Chem. Res. 57, 6576–6584. https://doi.org/10.1021/acs.iecr.8b00332.

Gonnella, G., Ischia, G., Fambri, L., Fiori, L., 2022. Thermal analysis and kinetic modeling of pyrolysis and oxidation of hydrochars. Energies 15, 950–970. https://doi.org/10.3390/en15030950.

Gromov, N.V., Medvedeva, T.B., Taran, O.P., Bukhtiyarov, A.V., Aymonier, C., Prosvirin, I.P., Parmon, V.N., 2018. Hydrothermal solubilization–hydrolysis–dehydration of cellulose to glucose and 5-hydroxymethylfurfural over solid acid carbon catalysts. Top. Catal. 61, 1912–1927. https://doi.org/10.1007/s11244-018-1049-4.

Güdücü, I., Alper, K., Evcil, T., Tekin, K., Ohtani, H., Karagöz, S., 2021. Effects of hydrothermal carbonization on products from fast pyrolysis of cellulose. J. Energy Inst. 99, 299–306. https://doi.org/10.1016/j.joei.2021.10.004.

Güleç, F., Samson, A., Williams, O., Kostas, E.T., Lester, E., 2022. Biofuel characteristics of chars produced from rapeseed, whitewood, and seaweed via thermal conversion technologies – impacts of feedstocks and process conditions. Fuel Process. Technol. 238, 107492. https://doi.org/10.1016/j.fuproc.2022.107492.

Guo, H., Qi, X., Li, L., Smith, Jr, R.L., 2012. Hydrolysis of cellulose over functionalized glucose-derived carbon catalyst in ionic liquid. Bioresour. Technol. 116, 355–359. https://doi.org/10.1016/j.biortech.2012.03.098.

Guo, H., Ogawa, S., Isoda, Y., Shen, F., Lee Smith, Jr, R., 2022. Weak-acid biochar catalyst prepared from mechanochemically-activated biomass and humic acid for production of 5-hydroxymethylfurfural. Biochar 4, 42–54. https://doi.org/10.1007/s42773-022-00170-1.

Hasdemir, İ.M., Yılmazoğlu, E., Güngör, S., Hasdemir, B., 2022. Adsorption of acetic acid onto activated carbons produced from hazelnut shell, orange peel, and melon seeds. Appl. Water Sci. 12, 271. https://doi.org/10.1007/s13201-022-01797-y.

Hornung, A., Stenzel, F., Grunwald, J., 2021. Biochar—just a Black Matter Is Not Enough. Biomass Convers. Biorefin. https://doi.org/10.1007/s13399-021-01284-5.

Huggins, T., Wang, H., Kearns, J., Jenkins, P., Ren, Z.J., 2014. Biochar as a sustainable electrode material for electricity production in microbial fuel cells. Bioresour. Technol. 157, 114–119. https://doi.org/10.1016/j.biortech.2014.01.058.

Igboke, O.J., Odejobi, O.J., Orimolade, T., Prevatt, G.H., Krishnan, S., 2023. Composition and Morphological Characteristics of Sulfonated Coconut Shell Biochar and its Use for Corncob Hydrolysis. Waste Biomass Valor. https://doi.org/10.1007/s12649-023-02080-0.

Iroba, K.L., Tabil, L.G., Sokhansanj, S., Dumonceaux, T., 2014. Pretreatment and fractionation of barley straw using steam explosion at low severity factor. Biomass

Bioenergy 66, 286–300. https://doi.org/10.1016/j.biombioe.2014.02.002.
Ischia, G., Cutillo, M., Guella, G., Bazzanella, N., Cazzanelli, M., Orlandi, M., Miotello, A., Fiori, L., 2022. Hydrothermal carbonization of glucose: secondary char properties, reaction pathways, and kinetics. J. Chem. Eng. 449, 13. https://doi.org/10.1016/j.cej.2022.137827.
Islam, M.T., Sultana, A.I., Chambers, C., Saha, S., Saha, N., Kirtania, K., Reza, M.T., 2022. Recent progress on emerging applications of hydrochar. Energies 15, 9340–9344. https://doi.org/10.3390/en15249340.
Kang, S., Li, X., Fan, J., Chang, J., 2012. Characterization of hydrochars produced by hydrothermal carbonization of lignin, cellulose, D-xylose, and wood meal. Ind. Eng. Chem. Res. 51, 9023–9031. https://doi.org/10.1021/ie300565d.
Kang, S., Ye, J., Zhang, Y., Chang, J., 2013. Preparation of biomass hydrochar derived sulfonated catalysts and their catalytic effects for 5-hydroxymethylfurfural production. RSC Adv. 3, 7360–7366. https://doi.org/10.1039/C3RA23314F.
Li, X., Tong, Z., Zhu, S., Deng, Q., Chen, S., Wang, J., Zeng, Z., Zhang, Y., Zou, J.-J., Deng, S., 2022. Water-mediated hydrogen spillover accelerates hydrogenative ring-rearrangement of furfurals to cyclic compounds. J. Catal. 405, 363–372. https://doi.org/10.1016/j.jcat.2021.12.010.
Licursi, D., Antonetti, C., Fulignati, S., Vitolo, S., Puccini, M., Ribechini, E., Bernazzani, L., Raspolli Galletti, A.M., 2017. In-depth characterization of valuable char obtained from hydrothermal conversion of hazelnut shells to levulinic acid. Bioresour. Technol. 244, 880–888. https://doi.org/10.1016/j.biortech.2017.08.012.
Lin, H., Zhang, L., Zhang, S., Li, Q., Hu, X., 2022. Hydrothermal carbonization of cellulose in aqueous phase of bio-oil: the significant impacts on properties of hydrochar. Fuel 315, 123132. https://doi.org/10.1016/j.fuel2022.123132.
Liu, J., Zhang, S., Jin, C., Shuang, E., Sheng, K., Zhang, X., 2019. Effect of swelling pretreatment on properties of cellulose-based hydrochar. ACS Sustain. Chem. Eng. 7, 10821–10829. https://doi.org/10.1021/acssuschemeng.9b01640.
Lu, X., Jordan, B., Berge, N.D., 2012. Thermal conversion of municipal solid waste via hydrothermal carbonization: comparison of carbonization products to products from current waste management techniques. Waste Manage. (Tucson, Ariz.) 32, 1353–1365. https://doi.org/10.1016/j.wasman.2012.02.012.
Ma, H., Yu, B., Yue, C., Qiao, Y., Li, N., Cai, T., Teng, J., 2023. Organocatalytic dehydration of fructose-based carbohydrates into 5-hydroxymethylfurfural in the presence of a neutral inner salt. ACS Omega 8, 16345–16355. https://doi.org/10.1021/acsomega.3c01111.
Masoumi, S., Borugadda, V.B., Nanda, S., Dalai, A.K., 2021. Hydrochar: a review on its production technologies and applications. Catalysts 11, 939. https://doi.org/10.3390/catal11080939.
Morales-Leal, F.J., Rivera de la Rosa, J., Lucio-Ortiz, C.J., De Haro-Del Rio, D.A., Solis Maldonado, C., Wi, S., Casabianca, L.B., Garcia, C.D., 2019. Dehydration of fructose over thiol– and sulfonic– modified alumina in a continuous reactor for 5–HMF production: study of catalyst stability by NMR. Appl. Catal. B Environ. 244, 250–261. https://doi.org/10.1016/j.apcatb.2018.11.053.
Paini, J., Benedetti, V., Ail, S.S., Castaldi, M.J., Baratieri, M., Patuzzi, F., 2022. Valorization of wastes from the food production industry: a review towards an integrated agri-food processing biorefinery. Waste Biomass Valorization 13, 31–50. https://doi.org/10.1007/s12649-021-01467-1.
Patwardhan, P.R., Satrio, J.A., Brown, R.C., Shanks, B.H., 2009. Product distribution from fast pyrolysis of glucose-based carbohydrates. J. Anal. Appl. Pyrolysis 86, 323–330. https://doi.org/10.1016/j.jaap.2009.08.007.
Pauline, A.L., Joseph, K., 2020. Hydrothermal carbonization of organic wastes to carbonaceous solid fuel – a review of mechanisms and process parameters. Fuel 279, 118472. https://doi.org/10.1016/j.fuel.2020.118472.
Plachy, T., Kutalkova, E., Skoda, D., Holcapkova, P., 2022. Transformation of cellulose via two-step carbonization to conducting carbonaceous particles and their outstanding electrorheological performance. Int. J. Mol. Sci. 23, 5477–5490. https://doi.org/10.3390/ijms23105477.
Popp, J., Kovács, S., Oláh, J., Divéki, Z., Balázs, E., 2021. Bioeconomy: biomass and biomass-based energy supply and demand. N. Biotech. 60, 76–84. https://doi.org/10.1016/j.nbt.2020.10.004.
Qi, X., Li, N., Lian, Y., 2015. Carbonaceous microspheres prepared by hydrothermal carbonization of glucose for direct use in catalytic dehydration of fructose. RSC Adv. 5, 17526–17531. https://doi.org/10.1039/c4ra15296d.
Qiao, Y., Theyssen, N., Hou, Z., 2015. Acid-catalyzed dehydration of fructose to 5-(hydroxymethyl)furfural. Recyclable Catalysis 2, 36–60. https://doi.org/10.1515/recat-2015-0006.
Ren, H., Cunha, E., Sun, Q., Li, Z., Kinloch, I.A., Young, R.J., Fan, Z., 2019. Surface functionality analysis by Boehm titration of graphene nanoplatelets functionalized via a solvent-free cycloaddition reaction. Nanoscale Adv. 1, 1432–1441. https://doi.org/10.1039/c8na00280k.
Reza, M.T., Rottler, E., Herklotz, L., Wirth, B., 2015. Hydrothermal carbonization (HTC) of wheat straw: influence of feedwater pH prepared by acetic acid and potassium hydroxide. Bioresour. Technol. 182. https://doi.org/10.1016/j.biortech.2015.02.024. 336–334. .
Saha, N., Saba, A., Reza, M.T., 2019. Effect of hydrothermal carbonization temperature on pH, dissociation constants, and acidic functional groups on hydrochar from cellulose and wood. J. Anal. Appl. Pyrolysis 137, 138–145. https://doi.org/10.1016/j.jaap.2018.11.018.
Saha, N., McGaughy, K., Reza, M.T., 2020. Elucidating hydrochar morphology and oxygen functionality change with hydrothermal treatment temperature ranging from subcritical to supercritical conditions. J. Anal. Appl. Pyrolysis 152, 104965. https://doi.org/10.1016/j.jaap.2020.104965.
Saleh, M., Isik, Z., Yabalak, E., Yalvac, M., Dizge, N., 2021. Green production of hydrochar nut group from waste materials in subcritical water medium and investigation of their adsorption performance for Crystal Violet. Water Environ. Res. 93, 3075–3089. https://doi.org/10.1002/wer.1659.
Saqib, N.U., Baroutian, S., Sarmah, A.K., 2018. Physicochemical, structural and combustion characterization of food waste hydrochar obtained by hydrothermal carbonization. Bioresour. Technol. 266, 357–363. https://doi.org/10.1016/j.biortech.2018.06.112.
Sasaki, M., Kabyemela, B., Malaluan, R., Hirose, S., Takeda, N., Adschiri, T., Arai, K., 1998. Cellulose hydrolysis in subcritical and supercritical water. J. Supercrit. Fluids 13, 261–268. https://doi.org/10.1016/S0896-8446(98)00060-6.
Sharma, H.B., Sarmah, A.K., Dubey, B., 2020. Hydrothermal carbonization of renewable waste biomass for solid biofuel production: a discussion on process mechanism, the influence of process parameters, environmental performance and fuel properties of hydrochar. Renew. Sustain. Energy Rev. 123, 109761. https://doi.org/10.1016/j.rser.2020.109761.
Sheng, K., Zhang, S., Liu, J., E, S., Jin, C., Xu, Z., Zhang, X., 2019. Hydrothermal carbonization of cellulose and xylan into hydrochars and application on glucose isomerization. J. Clean. Prod. 237, 117831. https://doi.org/10.1016/j.jclepro.2019.117831.
Solís, A., Rocha, S., König, M., Adam, R., Garcés, H.O., Candia, O., Muñoz, R., Azócar, L., 2023. Preliminary assessment of hazelnut shell biomass as a raw material for pellet production. Fuel 333, 126517. https://doi.org/10.1016/j.fuel.2022.126517.
Subratti, A., Vidal, J.L., Lalgee, L.J., Kerton, F.M., Jalsa, N.K., 2021. Preparation and characterization of biochar derived from the fruit seed of Cedrela odorata L and evaluation of its adsorption capacity with methylene blue. Sustain. Chem. Pharm. 21, 100421. https://doi.org/10.1016/j.scp.2021.100421.
Tamborini, L.H., Militello, M.P., Balach, J., Moyano, J.M., Barbero, C.A., Acevedo, D.F., 2019. Application of sulfonated nanoporous carbons as acid catalysts for Fischer esterification reactions. Arab. J. Chem. 12, 3172–3182. https://doi.org/10.1016/j.arabjc.2015.08.018.
Tsechansky, L., Graber, E.R., 2014. Methodological limitations to determining acidic groups at biochar surfaces via the Boehm titration. Carbon 66, 730–733. https://doi.org/10.1016/j.carbon.2013.09.044.
Volpe, M., Messineo, A., Mäkelä, M., Barr, M.R., Volpe, R., Corrado, C., Fiori, L., 2020. Reactivity of cellulose during hydrothermal carbonization of lignocellulosic biomass. Fuel Process. Technol. 206, 106456. https://doi.org/10.1016/j.fuproc.2020.106456.
Wang, K., Ye, J., Zhou, M., Liu, P., Liang, X., Xu, J., Jiang, J., 2017. Selective conversion of cellulose to levulinic acid and furfural in sulfolane/water solvent. Cellulose 24, 1383–1394. https://doi.org/10.1007/s10570-016-1184-7.
Wang, T., Zhai, Y., Zhu, Y., Li, C., Zeng, G., 2018. A review of the hydrothermal carbonization of biomass waste for hydrochar formation: process conditions, fundamentals, and physicochemical properties. Renew. Sustain. Energy Rev. 90, 223–247. https://doi.org/10.1016/j.rser.2018.03.071.
Wang, G., Dai, Y., Yang, H., Xiong, Q., Wang, K., Zhou, J., Li, Y., Wang, S., 2020. A review of recent advances in biomass pyrolysis. Energy Fuel. 34, 15557–15578. https://doi.org/10.1021/acs.energyfuels.0c03107.
Wiedner, K., Naisse, C., Rumperl, C., Pozzi, A., Wieczorek, P., Glaser, B., 2013. Chemical modification of biomass residues during hydrothermal carbonization—what makes the difference, temperature or feedstock? Org. Geochem. 54, 91–100. https://doi.org/10.1016/j.orggeochem.2012.10.006.
Wu, S., Wang, Q., Fang, M., Wu, D., Cui, D., Pan, S., Bai, J., Xu, F., Wang, Z., 2023. Hydrothermal carbonization of food waste for sustainable biofuel production: advancements, challenges, and future prospects. Sci. Total Environ. 897, 165327. https://doi.org/10.1016/j.scitotenv.2023.165327.
Xiong, X., Yu, I.K.M., Cao, L., Tsang, D.C.W., Zhang, S., Ok, Y.S., 2017. A review of biochar-based catalysts for chemical synthesis, biofuel production, and pollution

control. Bioresour. Technol. 246, 254–270. https://doi.org/10.1016/j.biortech.2017.06.163.
Xiong, X., Yu, I.K.M., Chen, S.S., Tsang, D.C.W., Cao, L., Song, H., Kwon, E.E., Ok, Y.S., Zhang, S., Poon, C.S., 2018. Sulfonated biochar as acid catalyst for sugar hydrolysis and dehydration. Catal. Today 314, 52–61. https://doi.org/10.1016/j.cattod.2018.02.034.
Xiros, C., Janssen, M., Byström, R., Børrosen, B.T., Cannella, D., Jørgensen, H., Koppram, R., Larsson, C., Olsson, L., Tillman, A.M., Wannstrom, S., 2017. Toward a sustainable biorefinery using high-gravity technology. Biofuel Bioproducts Biorefining 11, 15–27. https://doi.org/10.1002/bbb.1722.
Zhang, Y., Cao, Y., Yan, C., Liu, W., Chen, Y., Guan, W., Wang, F., Liu, Y., Huo, P., 2023. Rationally designed Au-ZrOx interaction for boosting 5-hydroxymethylfurfural oxidation. Chem. Eng. J. 459, 141644. https://doi.org/10.1016/j.cej.2023.141644.
Zhou, Z., Yao, D., Li, S., Xu, F., Liu, Y., Liu, R., Chen, Z., 2021. Sustainable production of value-added sulfonated biochar by sulfuric acid carbonization reduction of rice husks. Environ. Technol. Innov. 24, 102025. https://doi.org/10.1016/j.eti.2021.102025.
Zulfajri, M., Kao, Y.-T., Huang, G.G., 2021. Retrieve of residual waste of carbon dots derived from straw mushroom as a hydrochar for the removal of organic dyes from aqueous solutions. Sustain. Chem. Pharm. 22, 100469. https://doi.org/10.1016/j.scp.2021.100469.
Zuo, M., Niu, Q., Zhu, Y., Li, S., Jia, W., Zhou, Z., Zeng, X., Lin, L., 2023. Biochar catalysts for efficiently 5-Hydroxymethylfurfural (HMF) synthesis in aqueous natural deep eutectic solvent (A-NADES). Ind. Crop. Prod. 192, 115953. https://doi.org/10.1016/j.indcrop.2022.115953.